MICROCOPY RESOLUTION TEST CHART

NATIONAL BUREAU OF STANDARDS-1963-A

AD A138058

DEVELOPMENT AND FLIGHT TEST EVALUATION

OF AN ANALYTICAL MODEL OF THE

AIR-TO-AIR TRACKING TASK

THESIS

AFIT/GAE/AA/83S-2   William L. Eischen

DTIC
ELECTE
FEB 2 2 1984

A

DEPARTMENT OF THE AIR FORCE
AIR UNIVERSITY (ATC)

AIR FORCE INSTITUTE OF TECHNOLOGY

Wright-Patterson Air Force Base, Ohio

84 02 21 176

DEVELOPMENT AND FLIGHT TEST EVALUATION

OF AN ANALYTICAL MODEL OF THE

AIR-TO-AIR TRACKING TASK

THESIS

AFIT/GAE/AA/83S-2　　　William L. Eischens

Captain　　　USAF

FEB 2 2 1984

A

Approved for public release; distribution unlimited

AFIT/GAE/AA/83S-2

DEVELOPMENT AND FLIGHT TEST EVALUATION OF AN

ANALYTICAL MODEL OF THE AIR-TO-AIR TRACKING TASK

THESIS

Presented to the Faculty of the School of Engineering

of the Air Force Institute of Technology

Air University

in Partial Fulfillment of the

Requirements for the Degree of

Master of Science

by

William L. Eischens, B.S.

Capt   USAF

Graduate Aeronautical Engineering

September 1983

PREFACE

The essence of engineering is the ability to apply theory in a practical situation. This statement seems harmless enough but in reality can be the proverbial "bucket of worms"; it is a very difficult task. At times engineering becomes more of an art than a science. This is evident when we consider numbers used to make the theory match reality, technically referred to in engineering terms as "efficiency factors" or "proportionality constants." This thesis project highlighted some of the difficulties of aeronautical engineering. It started innocently enough as an attempt to determine an optimum roll axis for the air-to-air tracking task. This required adequately describing the dynamics of the attacking aircraft, target, and the relative kinematics between the two. The project ended with efforts to adequately describe the attacking aircraft dynamics, an effort that was initially supposed to be a minor portion of the overall project.

I owe debts of gratitude to many people and would like to acknowledge a few of them here. First of all to Captain Jim Silverthorn, who provided invaluable assistance throughout the project, upon numerous occasions explaining the finer points of the science part of engineering and providing enlightenment into the art of engineering. To Dr. Calico, for his assistance in setting up the project. Finally, to my classmates of USAF Test Pilot School Class

ii

82B, especially my test management project group members, Major Steve Heaps, Captains Steve Pitotti, Roger "Flash" Keith, and Ed Solski (Canada), and Lt. Samuel "Shmulik" Nehama (Israel). They put up with my unique style of leadership and were always ready to help.

Table of Contents

List of Figures

List of Tables

List of Symbols

Symbol	Description	Units
A_n	Normal acceleration	g, fps^2
An_T	Target normal acceleration	fps^2
b	Wing span	ft
c	Mean Aerodynamic Chord	ft
$C_L = L / \bar{q} S$	Lift Coefficient	
$C_D = D / \bar{q} S$	Drag Coefficient	
$C_m = M / \bar{q} S c$	Pitching moment coefficient	
$C_1 = L / \bar{q} S b$	Rolling moment coefficient	
$C_n = N / \bar{q} S b$	Yawing moment coefficient	
$C_y = F_y / \bar{q} S$	Side force coefficient	
$C_x = F_x / \bar{q} S$	Forward force coefficient	
$C_z = F_z / \bar{q} S$	Downward force coefficient	
$C_{1\delta}$	Variation of rolling moment coefficient with control surface angle	rad^{-1}
$C_{y\delta}$	Variation of side force coefficient with control surface angle	rad^{-1}
$C_{n\delta}$	Variation of yawing moment coefficient with control surface angle	rad^{-1}
g	Acceleration of gravity	ft/sec^2
I_{xx}, I_{yy}, I_{zz}	Moments of inertia about X, Y, Z axes, respectively	$slug/ft^2$
I_{xz}	Product of inertia in XYZ system	$slug/ft^2$
$C_{1\beta}$	Variation of rolling moment about X with sideslip angle	rad^{-1}
C_{1p}	Variation of rolling moment about X with roll rate	rad^{-1}
C_{1r}	Variation of rolling moment about X with yaw rate	rad^{-1}

m	Mass	slugs
$C_{m\alpha}$	Variation of pitching moment with angle of attack	rad^{-1}
$C_{m\dot{\alpha}}$	Variation of pitching moment with rate of change of angle of attack	rad^{-1}
C_{mq}	Variation of pitching moment with pitch rate	rad^{-1}
$C_{n\beta}$	Variation of yawing moment with sideslip angle	rad^{-1}
C_{np}	Variation of yawing moment with roll rate	rad^{-1}
C_{nr}	Variation of yawing moment with yaw rate	rad^{-1}
$C_{y\beta}$	Variation of side force with sideslip angle	rad^{-1}
C_{yp}	Variation of side force with roll rate	rad^{-1}
C_{yr}	Variation of side force with yaw rate	rad^{-1}
$\bar{q}$	dynamic pressure	lb_f/ft^2
S	Wing area	ft^2
U	Velocity along X	ft/sec
V	Velocity along Y	ft/sec
W	Velocity along Z	ft/sec
P,p	Roll rate	rad/sec
Q,q	Pitch rate	rad/sec
R,r	Yaw rate	rad/sec
Ψ,ψ	Heading angle	rad
Θ,θ	Pitch angle	rad
Φ,ϕ	Roll angle	rad
α	Angle of attack	rad

ix

β	Angle of sideslip	rad
ρ	Density	slugs/ft^3
	or	
	Roll axis depression angle	rad
$\dot{\beta}$	Derived sideslip rate	rad/sec
ϕ_c	Commanded bank angle	rad
ψ_T	Target heading angle	rad
θ_T	Target pitch angle	rad
ϕ_T	Target bank angle	rad
V_T	Target velocity	ft/sec
V_A	Attacker velocity	ft/sec
r_1, r_2, r_3	Relative distances of a target with respect to the attacker along the X, Y, and Z attacker axes respectively	ft
AFCS	Automatic Flight Control System	
CAS	Control Augmentation System	
DFCS	Digital Flight Control System	
HUD	Head Up Display	

ABSTRACT

A nonlinear simulation and a linear model are developed for
an air-to-air tracking task using the A-7D DIGITAC aircraft. The
nonlinear simulation includes the aircraft, flight control
system, and target dynamics, and the relative kinematics between
the aircraft and the target. The linear model represents the
linearized lateral-directional aircraft dynamics, the heading
angle, and the linearized lateral relative kinematics. The
models were used to describe the effect of depressing the
aircraft roll axis on the air-to-air tracking task using a fixed
gunsight.

A flight test program was conducted to determine the effects
of depressing the aircraft roll axis on the lateral-directional
dynamics and on the air-to-air tracking task. Open loop flight tests
were performed to determine the effect of depressing the roll axis on
the lateral-directional dynamics. (spiral, Dutch
roll, and roll mode tests, and lateral frequency sweeps) The
The most noticeable open loop effect of depressing the roll axis was
the decrease in roll mode time constant. Comparison of the
flight test and nonlinear model data showed good correlation for
both the mechanical flight control system and the standard
control augmentation system. The linear air-to-air tracking
model did not agree with flight test data due to lack of a
control system in the model. Size constraints of the linear
analysis program used, prevented incorporating the control system
system dynamics into the model.

Closed loop tracking tests were used to evaluate the effect of a depressed roll axis on the air-to-air tracking performance. The results of the evaluation showed that an effective roll axis depression angle equal to, or slightly more depressed than the fixed gunsight, were favored by the project pilots for the air-to-air tracking task.

I. INTRODUCTION

Substantial work has been done in the past with digital flight controls (References 1,2). The majority of the work was on optimizing the flight control laws for specific tasks. One task for which the flight controls were optimized, was that of air-to-air tracking with a fixed gunsight. The air-to-air tracking task has traditionally been the most difficult task in aerial combat. It requires precise fuselage pointing without adversely exciting gunsight/bullet stream dynamics. The air-to-air tracking task consists of two subtasks which are usually accomplished simultaneously. One is the longitudinal subtask of acquiring the proper lead on the target. The second is the lateral-directional subtask of getting into the target turning plane. This thesis considers the lateral-directional subtask and attempts to analytically describe it.

BACKGROUND

A YA-7D DIGITAC aircraft modified with a Digital Flight Control System (DFCS) has previously been used to investigate the effects of flight control law modifications on aircraft handling and task performance (References 1,2). This has led to the development and refinement of two multimodes, Precision Attitude (PA) and Flight Path (FP). The PA multimode is primarily concerned with controlling aircraft rates for precise fuselage pointing tasks such as air-to-air tracking. The FP multimode is

1

primarily concerned with controlling the aircraft velocity vector. In the longitudinal sense, the PA mode can be thought of as a pitch rate command system and the FP mode as a normal acceleration (g) command system. These two multimodes are not completely separate, as the PA mode blends into the FP mode for large amplitude aircraft maneuvers. The PA mode also contains a submode with provisions for depressing the effective aircraft roll axis by using the rudder to create a yaw rate proportional to the roll rate.

Previous DIGITAC tests showed better tracking results could be achieved by depressing the effective roll axis using the PA mode. Initial tests were designed to determine the "optimum" roll axis using a fixed depressed gunsight (Reference 3). This "optimum" roll axis was based upon pilot opinion and tracking performance. The results of the initial tests indicated the optimum roll axis was between 131 to 174 milliradians depression, for a two "g" target at 1500 feet range. Dynamic gunsights were then introduced (Reference 4). The tracking errors achieved with dynamic gunsights were about three times worse than with the fixed sight. This led to further testing with a dynamic sight to determine if a different "optimum" roll axis existed for the dynamic sight. Recent tests included the variation of other tracking variables, such as range, to determine their effect on the location of an "optimum" depressed roll axis (Reference 5). The test results indicated that the optimum depression angle for the roll axis, was at an angle greater than the sight depression

2

angle. However, the results did not isolate any one axis within this range as the "optimum."

OBJECTIVE

The objective of this thesis is to develop an analytical model of the air-to-air tracking task and compare it to flight test. If the air-to-air tracking task can be modelled as a linear closed loop control task, then conventional linear control analysis tools could be used to identify promising areas for flight test and increase the understanding of the flight test results achieved. There is a large knowledge base in the understanding of classical frequency domain design techniques which could be applied. If the air-to-air tracking task could be accurately modelled and represented on a locus and/or bode plots, then various configurations could be examined to determine their effects. The results could be used to guide flight test efforts.

APPROACH

This thesis develops a nonlinear simulation of the air-to-air tracking task, performs a linearized analysis, and then compares these models against flight test data. The models were developed starting with few assumptions. This permitted an estimate to be made of the errors as various simplifying assumptions were later introduced, and thereby provides a means

3

of determining the validity of the model. To accomplish a successful modelling effort for the air-to-air tracking task, the following steps were identified.

1. Develop a nonlinear simulation of the tracking task. This included six degree of freedom nonlinear aircraft dynamics, the flight control system, target dynamics, and the relative kinematics between the target and the aircraft. This step was to establish the baseline against which all further assumptions were to be compared. The nonlinear simulation incorporates fewer assumptions compared to any of the linear simulations. This becomes important when attempting to describe a complex task which may contain important nonlinear effects. The nonlinear simulation would have the highest probability of accurately describing the actual task dyanmics.

2. Describe the tracking task with linearized equations using state variables. This will allow the use of conventional linear analysis tools (ie. Root Locus), in analyzing the task.

3. Validate the models. This means comparing the aircraft and flight control model data with flight test data. This was to be accomplished with open loop (no "pilot in the loop") tests.

4. Evaluate the ability of the models to describe the air-to-air tracking task. This is the final step, which combines the target dynamics and relative kinematics with the validated aircraft and flight control system. This was to be accomplished with closed loop ("pilot in the loop") tracking tests.

To limit the scope of this project to a managable level, only the effect of depressing the roll axis of the aircraft on

the air-to-air tracking task was considered. The modelling effort will consider the aircraft at one flight condition with fixed target range and simple, cooperative target, maneuvers. The target range was fixed at 1500 feet since that is approximately the "normal" range for air-to-air gunnery, giving a bullet time of flight of less than a second. The fixed range in combination with a fixed depressed sight and a constant g target, results in a constant depression difference between the aircraft roll axis and the sight. Thus, the effect of a change in roll axis depression on the tracking task can be evaluated without the complexity of additional variables.

SIGN CONVENTION .

The following sign convention is used throughout this project.

    1. The positive axes and forces are out the nose for the X axis, out the right wing for the Y axis, and down for the Z axis.

    2. The positive moments are pitch up, roll right, and yaw right.

    3. The positive control surface movements are elevator trailing edge down, right aileron up, and rudder trailing edge left.

    4. The positive pilot control inputs are stick back, stick right, and rudder left.

5

II. DEVELOPMENT OF THE NONLINEAR EQUATIONS

The first step in performing a system performance analysis
is to adequately describe the system. This chapter presents a
description of the aircraft, control system, and air-to-air
tracking task and a description of the nonlinear differential
equations used to model these dynamics.

AIRCRAFT DESCRIPTION

The A-7D aircraft is a subsonic, single-seat, land based
light attack airplane powered by a single Allison TF-41-A-1
turbofan engine rated at 14,250 pounds thrust without
afterburning. The swept wing is mounted high on the fuselage
with a slight anhedral. The wing control surfaces include plain
sealed inset ailerons, spoilers, leading edge flaps, and single
slotted trailing edge flaps. The tail has a swept vertical fin,
rudder, and an all moveable horizontal stabilizer.

A-7 DYNAMICS

The flight condition selected for this study was a cruise
configuration at 15,000 feet pressure altitude and 0.6 Mach.
This is a flight condition for which aircraft data was readily
available. Aircraft data for this configuration is tabulated in
Table 1. Some of the primary assumptions used in developing the
equations of motion were:

6

1. The X and Z axes are in the plane of symmetry and the origin of the axes is at the center of gravity of the aircraft.

2. The mass of the aircraft is constant.

3. The aircraft is a rigid body.

4. The flat earth approximation is appropriate.

5. The flow is quasi-steady.

The A-7 aircraft was considered as a three dimensional body with six degrees of freedom, three translational and three rotational. A set of nonlinear coupled ordinary differential equations were used to describe the aircraft. Reference 7 by Roskam was used as the source of the equations. The equations are shown in tables 2, 3, and 4. These equations were written for the aircraft body axes. Straight and level flight was assumed for initial conditions.

TABLE I

A-7D Cruise Configuration Data

(Reference 6)

Altitude	h	15,000 feet PA
Mach No.	M	0.6
Weight	W	25,338 lbs
Center of Gravity	CG	28.7% MAC
Dynamic Pressure	$\bar{q}$	300 slugs/sq ft
Wing Area	S	375 sq ft
Wing Span	b	38.73 ft
Mean Aero Chord (MAC)	c	10.84 ft
Moment of Inertia	I_{xx}	15,365 slugs sq ft
Moment of Inertia	I_{yy}	69,528 slugs sq ft
Moment of Inertia	I_{zz}	79,005 slugs sq ft
Product of Inertia	I_{xz}	-1,664 slugs sq ft

8

TABLE II

NONLINEAR AIRCRAFT EQUATIONS

A/C FORCE EQUATIONS

$$\dot{U} = VR - (W+W_0)Q - g \sin \theta + \bar{q}SC_x/m + T/m$$

$$\dot{V} = (W+W_0)P - UR + g \sin \phi \cos \theta + \bar{q}SC_y/m$$

$$\dot{W} = UQ - VP + g \cos \phi \cos \theta + \bar{q}SC_z/m$$

A/C MOMENT EQUATIONS

$$\dot{P} = I_1 P Q - I_2 Q R + I_3 \bar{q} S b C_1 + I_4 \bar{q} S b C_n$$

$$\dot{Q} = -I_5 P R - I_6 (P^2-R^2) + I_7 \bar{q} S c C_m$$

$$\dot{R} = I_8 P Q - I_9 Q R + I_{10} \bar{q} S b C_1 + I_{11} \bar{q} S b C_n$$

A/C KINEMATIC EQUATIONS

$$\dot{\phi} = P + Q \sin \phi \tan \theta + R \cos \phi \tan \theta$$

$$\dot{\theta} = Q \cos \phi - R \sin \phi$$

$$\dot{\psi} = Q \sin \phi / \cos \theta + R \cos \phi / \cos \theta$$

$$\alpha \cong W / (U^2 + V^2 + W^2)^{1/2}$$

$$\beta \cong V / (U^2 + V^2)^{1/2}$$

TABLE III

INERTIAL TERM EQUATIONS

$$I_1 = [1-(I_{yy}-I_{xx}/I_{zz})]/[(1-(I_{xz}^2/I_{xx}I_{zz}))]$$

$$I_2 = [I_{xz}^2/I_{xx}I_{zz} + (I_{zz}-I_{yy}/I_{xx})] / [1-(I_{xz}^2/I_{xx}I_{zz})]$$

$$I_3 = (1/I_{xx})/ [1-(I_{xz}^2/I_{xx}I_{zz})]$$

$$I_4 = (I_{xz}/I_{xx}I_{zz}) / (1-I_{xz}^2/I_{xx}I_{zz})$$

$$I_5 = (I_{xx}-I_{zz}) / I_{yy}$$

$$I_6 = I_{xz} / I_{yy}$$

$$I_7 = 0.5 I_{yy}$$

$$I_8 = [I_{xz}^2/I_{xx}I_{zz} - (I_{yy}-I_{xx} / I_{zz})] / [1-I_{xz}^2/I_{xx}I_{zz}]$$

$$I_9 = I_{xz}/I_{zz} ([1+(I_{zz}-I_{yy} / I_{xx})] / [1-I_{xz}^2/I_{xx}I_{zz}])$$

$$I_{10}= (I_{xz}/I_{xx}I_{zz}) / (1-I_{xz}^2/I_{xx}I_{zz})$$

$$I_{11}= (1/I_{zz}) / (1-I_{xz}^2/I_{xx}I_{zz})$$

TABLE IV

AERODYNAMIC DERIVATIVES

$$C_L = C_{LO} + C_{L\alpha}\alpha + C_{L\dot\alpha}\,\dot\alpha c/2U + C_{Lq}\;qc/2U + C_{L\delta e}\,\delta e$$

$$C_D = C_{DO} + k\,C_L^2$$

$$C_x = C_L\,\sin\alpha - C_D\,\cos\alpha$$

$$C_y = C_{y\beta}\,\beta + C_{yp}\,pb/2U + C_{yr}\,rb/2U + C_{y\delta a}\,\delta a + C_{y\delta r}\,\delta r$$

$$C_z = -C_D\,\sin\alpha - C_L\,\cos\alpha$$

$$C_1 = C_{1\beta}\,\beta + C_{1p}\,pb/2U + C_{1r}\,rb/2U + C_{1\delta a}\,\delta a + C_{1\delta r}\,\delta r$$

$$C_m = C_{m\alpha}\,\alpha + C_{m\dot\alpha}\,\dot\alpha c/2U + C_{mq}\,qc/2U + C_{m\delta e}\,\delta e$$

$$C_n = C_{n\beta}\,\beta + C_{np}\,pb/2U + C_{nr}\,rb/2U + C_{n\delta\epsilon}\,\delta a + C_{n\delta r}\,\delta r$$

$$A_n = -qSC_z/m$$

$$Ay = qSC_y/m$$

$$k = 1 / \;ARe \qquad e = \text{Oswald's efficiency factor} - 0.8$$

$$= 0.0194$$

CONTROL SYSTEM DYNAMICS

The A-7D DIGITAC DFCS duplicates the standard A-7 Control
Augmentation System (CAS) and in addition provides two pilot
selectable multimodes, Precision Attitude (PA) and Flight Path
(FP). The PA mode is used to depress the effective roll axis of
the aircraft. Appendix A gives a more detailed description of
the flight control system. Thus, the pilot has a choice of three
flight control setups: mechanical only, mechanical plus CAS, and
mechanical plus multimode.

The A-7D CAS was modelled with differential equations that,
when coupled to the A-7 dynamics equations, provide the control
surface inputs. The model includes both the mechanical and CAS
systems from the pilot force input to the control surface
deflections. The control system block diagrams are shown in
Figures 1 and 2 (Reference 8). It was necessary to include the
mechanical system since the CAS is only partial authority. The
CAS is connected to the mechanical system through a series servo
(mechanical adder) and provides control input shaping. The
dynamics of the rate gyros and series servos were not considered
significant and were not modelled.

The elevator axis contains both pitch rate and normal
acceleration feedback through the DFCS from rate and acceleration
sensors. In addition, bobweights within the mechanical system
also sense pitch acceleration and normal acceleration which
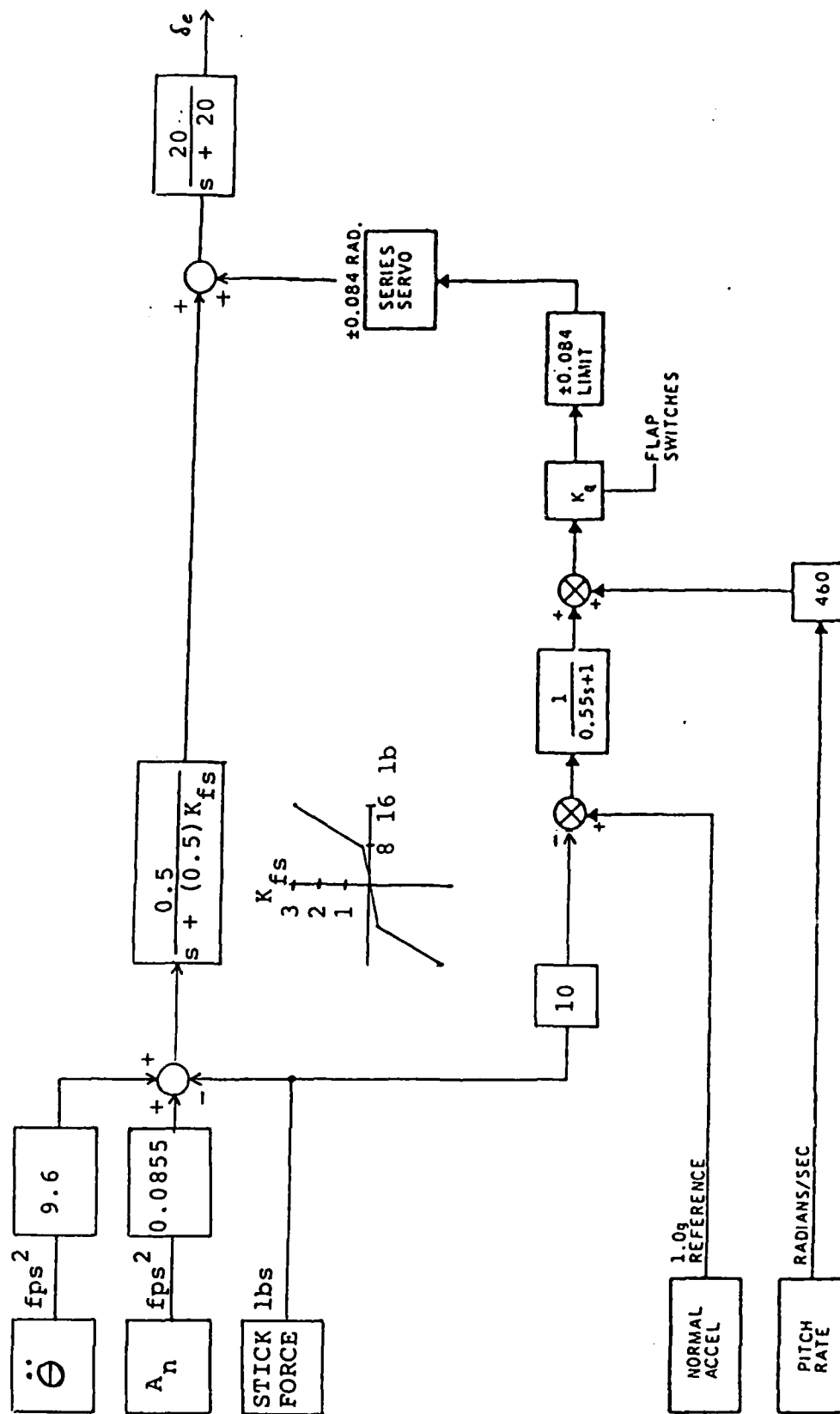provides a mechanical feedback of these variables to the elevator
surface.

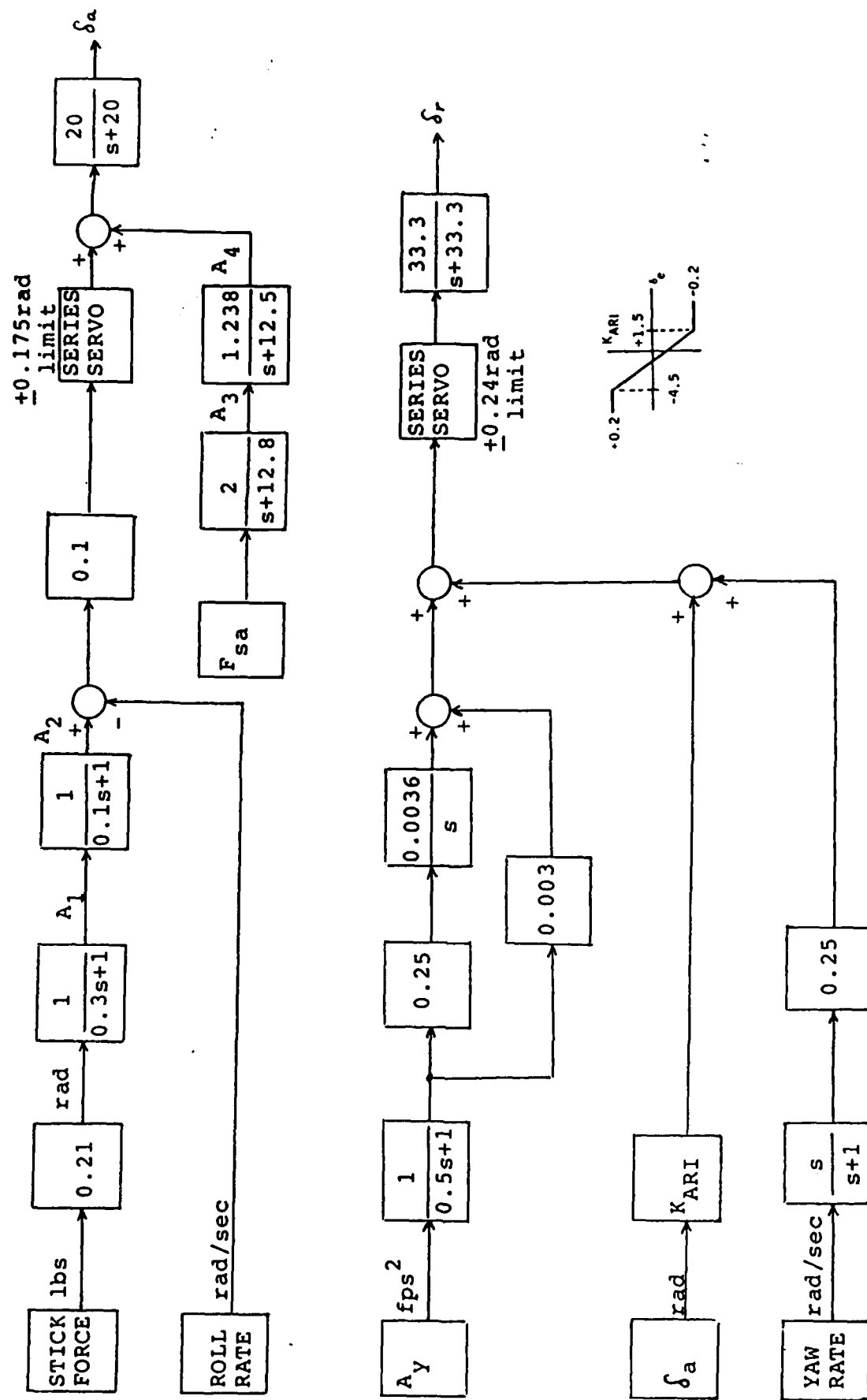FIGURE 1: MECHANICAL AND CAS – PITCH AXIS

13

FIGURE 2: MECHANICAL AND CAS ROLL AND YAW AXES

14

The roll axis CAS has roll rate feedback through the DFCS as well as pilot lateral stick inputs. In addition, the mechanical path contains a feel spring, viscous damper, and roll isolation servo, all of which has a significant effect on the roll dynamics of the aircraft.

The mechanical rudder system is a simple gain. The yaw CAS has side acceleration and yaw rate feedbacks and an aileron to rudder interconnect scheduled with elevator position.

The PA rudder system (Appendix A) has side acceleration and derived sideslip rate feedbacks and an aileron to rudder interconnect scheduled with angle of attack. One of the principal features of the PA mode is that various effective roll axes can be obtained. This is done by modifying the sideslip rate feedback as shown below. Estimated sideslip rate is derived from the equation:

$$\dot{\beta} = p\alpha - r + (g/U) \sin \phi \cos \theta \qquad [1]$$

For a normal coordinated turn, $\dot{\beta}$ should be zero. Feeding this back to the rudder creates a yaw rate into the direction of the roll. This tends to minimize the amount of sideslip generated during rolling maneuvers, by effectively depressing the roll axis to be aligned with the aircraft's velocity vector. That is, the yaw rate combined with roll rate results in an depressed roll axis according to the approximation:

$$\rho = r / p \qquad [2]$$

where ρ is the roll axis depression angle and both r and p are measured in the body axes. Depression of the roll axis beyond

15

the velocity vector is achieved by replacing the angle of attack term in the above equation (which represents the depression of the velocity vector), by a fixed angle term (Kp_α), representing the desired depression of the roll axis. For example, $Kp_\alpha = 0.1$ would tend to produce an effective roll axis 0.1 radians depressed from the fuselage reference line.

AIR-TO-AIR TRACKING TASK

The air-to-air tracking task is one of positioning the attacking aircraft behind the target and in the target turning plane with the proper lead so as to place a gunsight on the target and maintain it there. The gunsight approximates the location of a bullet one time of flight after being fired from the attacking aircraft. The gunsights range from a sight fixed with respect to the aircraft to an undamped sight which represents the true bullet stream dynamics.

There are generally two phases to the air-to-air tracking task. First is the gross acquisition phase where the attacking aircraft is maneuvered without reference to the sight into the general position necessary for tracking. At this point the aircraft would be close to the target turning plane, approximately 1500 to 2500 feet in trail near to the appropriate lead angle. Then the second, or fine tracking, phase starts where the sight is now referenced in attempting to correct both the lateral and longitudinal errors between the sight and target. Pitch corrections are used to zero longitudinal errors and roll

16

corrections along with some rudder are used for lateral errors. Discussions with pilots experienced in air-to-air tracking, led to the impression that to correct for lateral errors, the pilot would first match his bank angle to the target, determine the lateral error, then adjust the bank angle to fly into the target turning plane. The sight was not precisely used whenever the attacking aircraft bank angle did not match the target's due to pendulum effect.

Pendulum effect occurs whenever the aircraft is rolled and the sight axis is different than the aircraft roll axis. When the roll axis is above the sight (the normal situation) , the sight will appear to move away from the target when the aircraft is rolled towards the target. This is depicted as adverse pendulum effect in Figure 3. In this example, the pilot must roll right in order to translate over to the target's turning plane. In so doing, however, the gunsight will appear to move to the left, initially increasing the perceived lateral error. This gives the pilot a false indication of the magnitude of the lateral error and does not provide a cue as to when to roll out. This can lead to sight oscillation about the target as the pilot tries to guess when his roll axis is in the target turning plane. The opposite effect is achieved when the roll axis is below the sight. In this case the sight will appear to move toward the target as the pilot rolls toward the target. Once the sight is on the target, the pilot keeps it there and, in theory at least, it will lead him into the target turning plane. A third situation occurs when the roll axis is at the sight. Here, for a
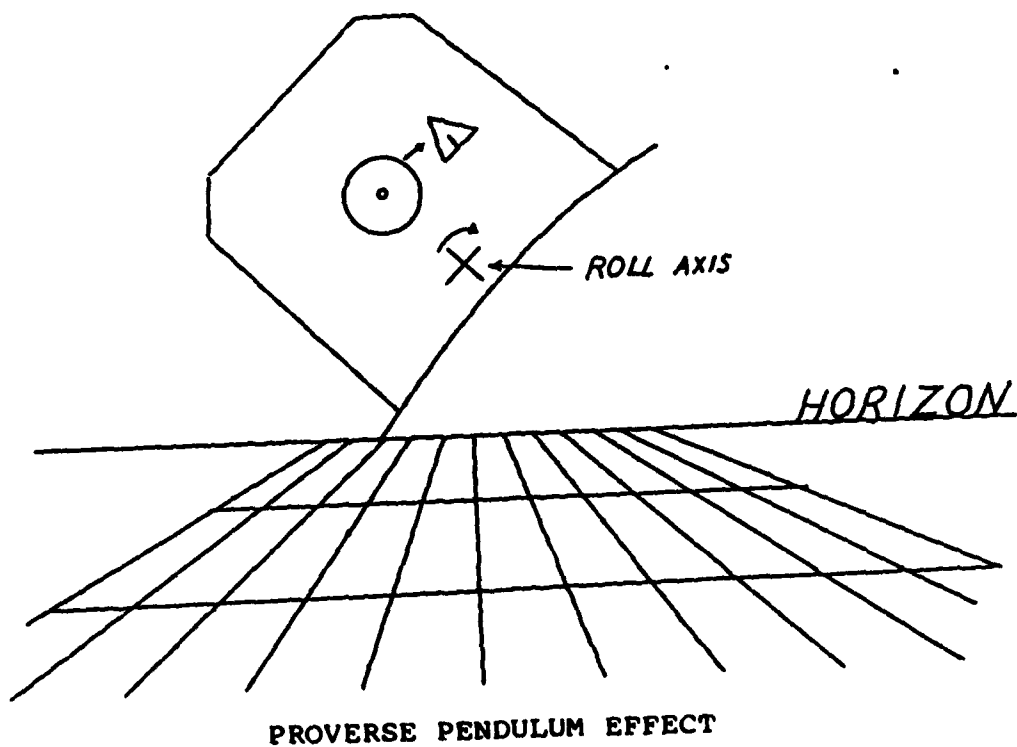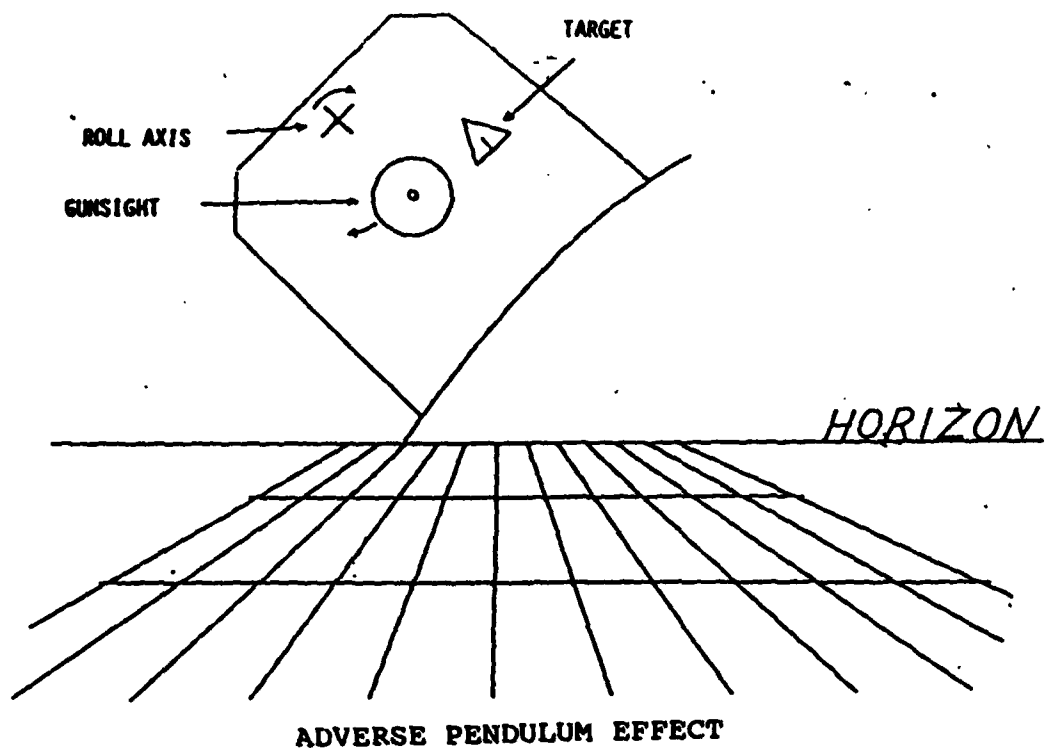
17

ADVERSE PENDULUM EFFECT

PROVERSE PENDULUM EFFECT

FIGURE 3: PENDULUM EFFECT

18

fixed sight, there would be no pendulum effect and the sight could be flown to wherever it needed to be. In practice, a computing sight would take gravity drop into account which would cause the sight to be off the aircraft centerline. This would cause a pendulum effect where an attempt to correct a lateral error by rolling would create an indication of both a longitudinal and lateral error.

This pendulum effect caused by the location of the roll axis is what led to the present investigations into the possible existence of one "optimum" roll axis. In this thesis, only the lateral fine tracking task with a fixed sight was examined. The longitudinal task was eliminated to simplify the analysis. The fixed sight was used because with a dynamic gunsight it is difficult, if not impossible, to distinguish aircraft dynamics from gunsight dynamics during analysis and flight testing.

Since the thesis is dealing with a fixed sight, the task of analytically representing the air-to-air tracking situation became simply one of describing the motion of the target with respect to the attacking aircraft.

The target was represented as a point mass performing a constant speed, constant "g", turn. The following equations represent the target performing such a maneuver, where V_T is the target speed, and the angles ψ_T and θ_T describe the target direction. Target bank angle (ϕ_T) was included for reasons discussed previously.

19

$$\dot{V}_T = 0$$

$$\dot{\psi}_T = A_{nT} \sin \phi_T / V_T \cos \theta_T$$

$$\dot{\theta}_T = (A_{nT} \cos \phi_T - g \cos \theta_T) / V_T$$

$$\dot{\phi}_T = P_T$$

$$A_{nT} = g / \cos \phi_T \quad \text{(for a level turn)} \qquad [3]$$

The relative kinematics between the target and attacking aircraft were described by referencing both the target and attacking aircraft to an earth fixed reference frame, then transforming them back up to the aircraft body reference frame. Figure 4 illustrates and Appendix C shows the equation development.

NONLINEAR SIMULATION

This chapter presented the development of the aircraft equations of motion, control system dynamics, target dynamics, and relative kinematics between the target and the aircraft. These equations and the understanding of the air-to-air tracking task presented in this chapter forms the basis for the air-to-air tracking simulation.

The simulation uses a fourth order Runge-Kutta with an integration interval of 0.05 seconds to solve the differential equations. The 0.05 second interval was necessary due to the fast rudder actuator. The simulation went unstable with a larger

20
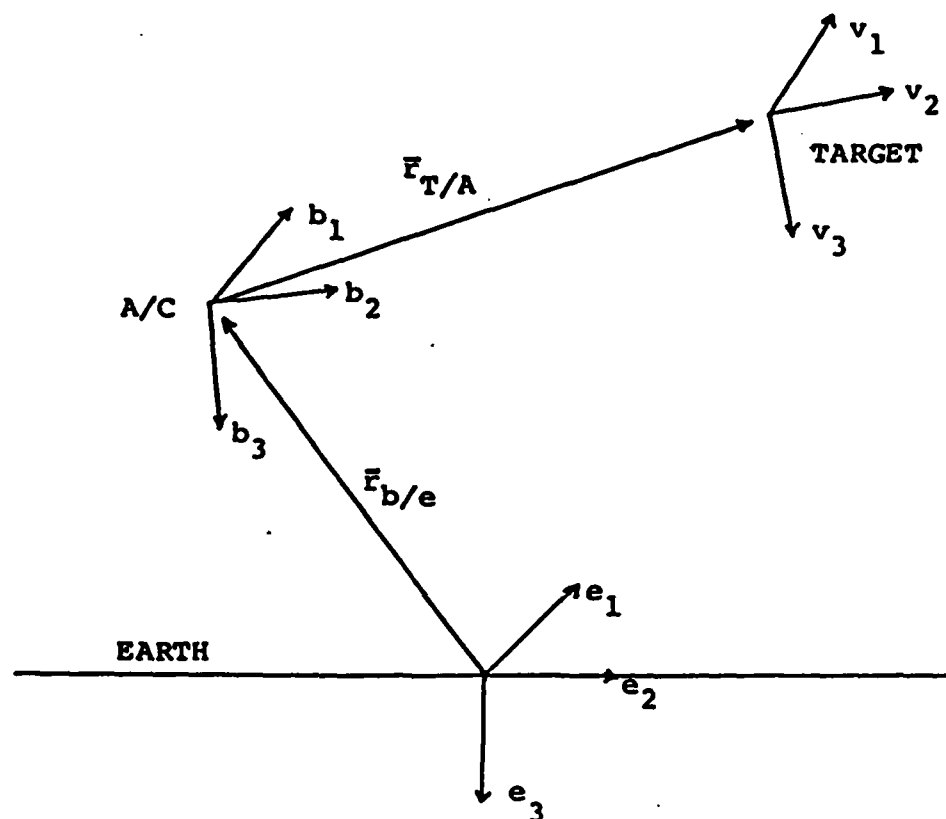
$$\frac{^b d}{dt} (\bar{r}_{T/A}) = -(\bar{w}^{be} \times \bar{r}_{T/A}) + \bar{V}_T - \bar{V}_A$$

$$
\begin{bmatrix} \dot{r}_1 \\ \dot{r}_2 \\ \dot{r}_3 \end{bmatrix} = - \begin{bmatrix} 0 & -R & Q \\ R & 0 & -P \\ -Q & P & 0 \end{bmatrix} \begin{bmatrix} r_1 \\ r_2 \\ r_3 \end{bmatrix} + [C^{be}][C^{ev}] \begin{bmatrix} V_T \\ 0 \\ 0 \end{bmatrix}_v - \begin{bmatrix} U \\ V \\ W \end{bmatrix}_b \qquad [4]
$$

FIGURE 4:   RELATIVE KINEMATICS

interval (0.1 second), while no difference in results were obtained with a smaller interval (0.025 seconds). The entire simulation was coded in the Pascal language to allow it to be executed on a microcomputer. The flow of events for the simulation are shown in Figure 5.

In the simulation, the angle of attack, pitch attitude, and elevator deflection represent perturbations away from nonzero trim values, although the trim values are assumed zero, whereas the other variables (excluding U) have true zero initial conditions. This is not really a problem for longitudinal maneuvering, but for lateral-directional maneuvering the problem becomes especially evident in the $\dot{V}$ equation. There will always be an initial W velocity in the body axes if the aircraft is at an angle of attack. The generation of a roll rate will therefore create a value which will cancel the value created by the yaw rate and the aircraft will effectively roll about the aircraft velocity vector (i.e. normal coordination). Since a zero W initial velocity was assumed, that does not happen and a false side velocity is generated which causes problems with the flight control system feedbacks which attempted to cancel the side velocity. The solution was to include an initial W term in the $\dot{V}$ and $\dot{U}$ equations. In the $\dot{V}$ equation it has no effect as long as there is no roll rate, but creates a nonzero term once a rolling motion starts, which is the desired effect. The effect of the initial W in the $\dot{U}$ equation is similar for pitch rate.
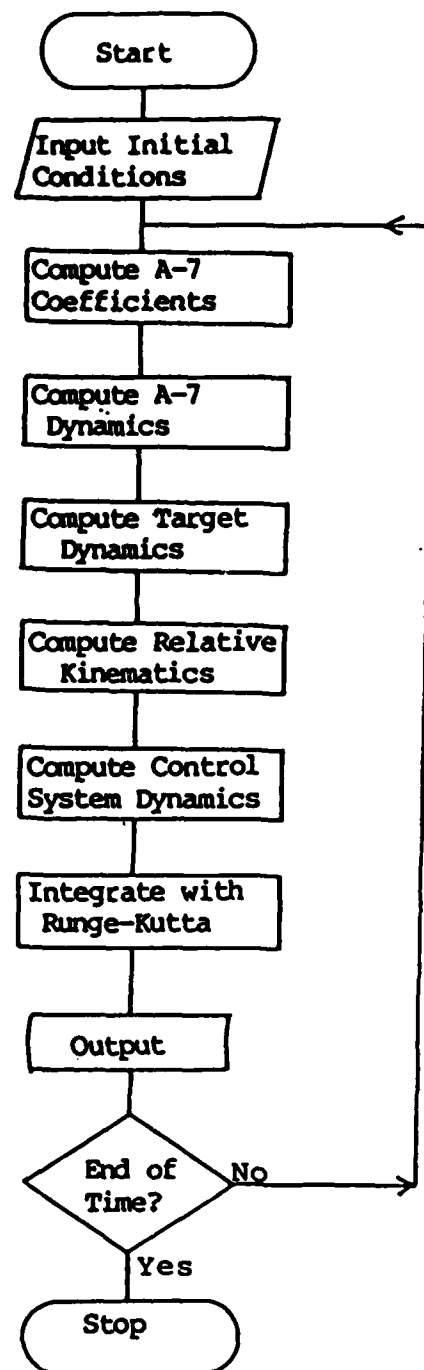
FIGURE 5: SIMULATION FLOW CHART

The thrust is assumed to be fixed at the correct value for the trim condition. The correct value is when the thrust balances the total drag. The C_{LO} in the lift equation is not the zero angle of attack lift coefficient, but is instead the lift coefficient at the trim condition.

The inputs were the initial values for the state variables (only U, V_T, and r_1 were required, all others were assumed zero), pilot lateral stick and rudder force and the starting and ending times for the simulation (generally zero start time). The outputs were all 28 state variables, normal acceleration, target normal acceleration, lateral sight error, longitudinal sight error, side acceleration angle of attack, sideslip angle, each as a function of time.

The output variables were stored in a disk file while the program was executing. A separate program was used to print out 16 of the variables to a line printer. The output file could also be used to generate a plot of any output variable versus time through a separate plot program. The plot was done on a dot matrix printer. Appendix B contains a listing of the simulation program and print program.

III. DEVELOPMENT OF LINEAR ANALYSIS

The development of the nonlinear simulation provides the baseline against which the validity of a linear model can be checked. The linear model provides the proper representation of the air-to-air tracking task for using linear control analysis tools (i.e. Root Locus). The linear analysis program used (TOTAL, Reference 9), could only handle up to a tenth order system when using the state variable setup, thus limiting the size of the linear model. The nonlinear model was 28th order. Therefore, the problem must be simplified more than by the standard linearizing assumptions. The complexity of the flight control system precluded being able to reduce the linear system to the tenth order. Other linear analysis methods could have been used which would have allowed a higher order linear system analysis, however, they would have limited the ability to make changes to the model or to examine other outputs from the model. The flexibility of the state variable approach was a significant and highly desirable advantage although the size constraints of this approach proved to be a major barrier in this thesis.

Although the aircraft response could not be adequately represented in reduced order linear form, a preliminary linear analysis of the air-to-air tracking task portrayed an interesting phenomena. The following development of the preliminary linear model is presented as an introduction to the phenomena noted.

The preliminary linear model represented the air-to-air tracking task in state variable form. Six state variables were

25

originally used. Four were the usual lateral-directional

aircraft state variables (v, p, r, ϕ). Additionally, the heading

angle (ψ), was included and the lateral relative kinematic

equation was also used.

From Equation [4]:

$$\dot{r}_2 = -Rr_1 + Pr_3 + V_T \left[(\cos \psi_T \cos \theta_T)(\cos \psi \sin \phi \sin \theta - \sin \psi \right.$$
$$\cos \phi) + (\cos \theta_T \sin \psi_T)(\sin \psi \sin \phi \sin \theta + \cos \psi \cos \phi)$$
$$\left. - \sin \theta_T \cos \theta \sin \phi \right] - V$$

Assuming $\quad r_1 = $ constant $\quad\quad \psi_T = 0 \quad\quad \theta_T = 0$

$$\psi = \Delta\psi \quad\quad\quad \psi_o = 0$$

$$\phi = \Delta\phi \quad\quad\quad \phi_o = 0$$

$$\theta = \Delta\theta \quad\quad\quad \theta_o = 0$$

and higher order perturbation terms can be neglected, one

obtains:

$$\dot{r}_2 = -rr_1 + pr_3 + V_T(-\psi) - v \quad\quad\quad\quad [5]$$

Combining this with the linear equations obtained from

Roskam (Ref 7) one obtains the sixth order state variable

representation of the lateral-directional aircraft dynamics and

lateral relative kinematics. The value of N_r' in these equations

was artificially increased to approximate a yaw stability

augmentation system (SAS). This avoided modelling the entire yaw

axis control system with all its associated dynamics. This

produced a well damped $(\zeta = 0.5)$ dutch roll mode as would be

expected. Next, a roll attitude feedback loop was added which

approximated the inner loop dynamics of a pilot, since most

pilots can rapidly close a roll attitude loop. The effect of the

26

roll attitude loop is to couple the roll and spiral roots

together and move them outside of the dutch roll roots (figure

6). This results in the preliminary state variable

representation of the air-to-air tracking task which now takes

the form:

$$\dot{\bar{x}} = [A]\bar{x} + [B]\bar{u}$$

where $\bar{x}^T = [v \ p \ r \ \phi \ \psi \ r_2]$ and $u = \phi_c$. Appendix D shows the

linear model development and the A and B matrices.

This linear representation does not include any control

system or target dynamics. This model also represents the

depressed roll axis effect by positioning the target above and

below the normal aircraft roll axis (adjust the r_3 term). A

better and more accurate way to describe the effect of depressing

the roll axis on the air-to-air tracking task is to include the

control system dynamics, this would then represent the actual

means of depressing the roll axis and also the effect of the

control dynamics on aircraft handling and the tracking task. But

as described before, limitations in the control system analysis

program prohibited this.

The results of the preliminary linear analysis are shown on

a root locus plot in Figures 6 and 7. These figures represent

the closed loop poles that would result if the pilot fed back

lateral position error (r_2) to ϕ_c. Figure 6 represents a roll

axis elevated 50 milliradians above the target while figure 7

represents a 25 milliradian depressed roll axis below the target.

The location of a pair of complex zeros close to the dutch roll

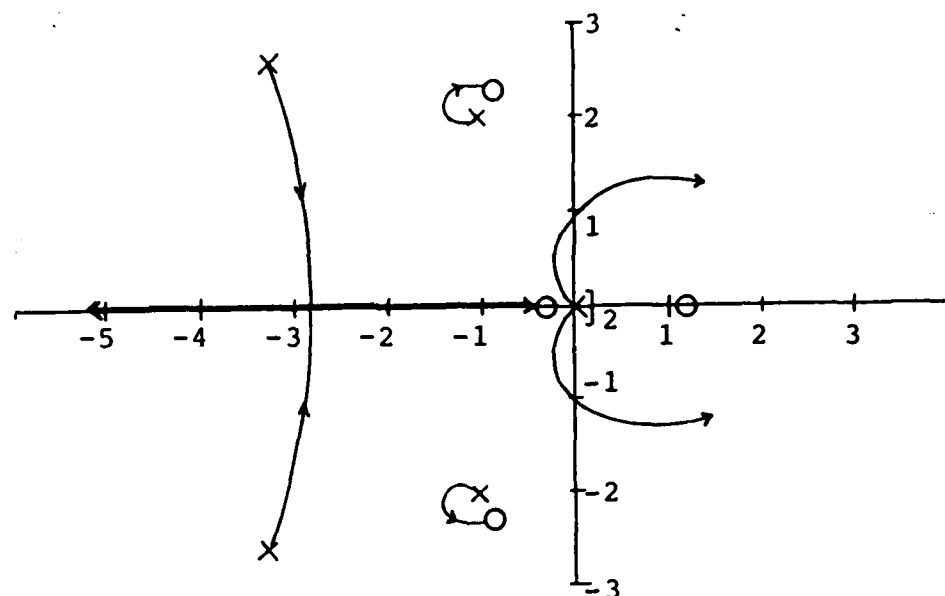poles effectively eliminates the dutch roll in the lateral

27

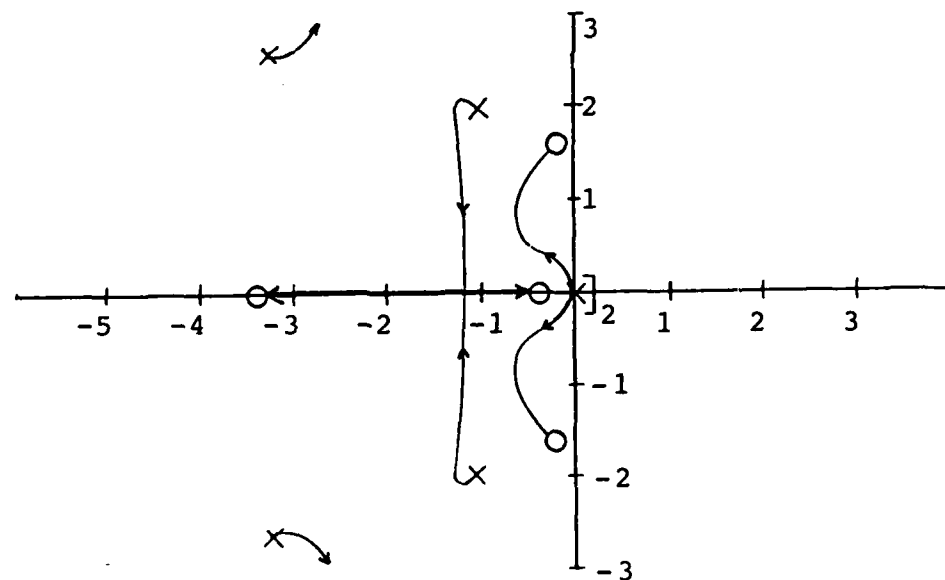FIGURE 6: r_2 VS ϕ_c ROOT LOCUS - 72 MIL DEPRESSION

FIGURE 7: r_2 VS ϕ_c ROOT LOCUS - 147 MIL DEPRESSION

28

position error dynamics. The interesting phenomena noted with
the effective depression of the roll axis is the movement of a
zero on the real axis. It starts from near zero on the positive
axis and moves to the right as the roll axis is depressed. The
zero wraps around from plus infinity to minus infinity as the
roll axis reaches the sight depression and moves in on the
negative real axis as the roll axis is depressed further than the
sight. This intuitively appears to be the correct movement since
a zero in the right half s plane indicates an initial time
response in the opposite direction of final movement. In this
case, this corresponds to an initial increase in lateral error
caused by the adverse pendulum effect. The switch from positive
to negative real axis also occurs when the sight goes from
adverse to proverse pendulum effect.

A preliminary hypothesis was formed which considered the
zero location as an indication of the pilot lead required. If
the pilot were to react as a simple gain in feeding lateral
position error back to a bank angle command, then the 72 mil
depression would yield a lightly damped response, while the 147
mil depression would give relatively good damping. To increase
the damping, the pilot would have to add lead to draw the root
locus to the left. The further out on the negative real axis (or
in on the positive axis) the roll axis depression zero was,
indicated more pilot lead was required. Pilot lead was equated
to pilot compensation required. Increasing the compensation
(increase lead) required, increases the pilot workload and
generally results in poor pilot ratings.

29

IV. THE FLIGHT TEST PROGRAM

The flight test program was designed to validate the nonlinear model and then evaluate the ability of the linear model to describe the air-to-air tracking task. Five depressed roll axes, equally spaced from 72 to 172 mils depression from the fuselage reference line, were used for both the validation and evaluation phases. A fixed gunsight at 122 mils depression was used for the tracking evaluation. Open loop (no "pilot in the loop") tests were done to validate the nonlinear model. Closed loop ("pilot in the loop") tests were done to evaluate the linear model. The following sections contain excerpts from the flight test report (Reference 10) and explain the test objectives, methods, and results.

TEST OBJECTIVES

OPEN LOOP OBJECTIVES

The general open loop testing objective was to provide data to determine if the analytical model adequately described the actual aircraft lateral-directional dynamics. To achieve this, lateral-directional characteristics were determined for the baseline unaugmented A-7D, normally augmented A-7D, and each of the five depressed roll axes. Specific tests included determination of the Dutch roll, roll, and spiral mode

30

characteristics. In addition, the frequency response characteristics of the DIGITAC aircraft were evaluated at specific points in the test envelope and compared with linear model derived results. The results of the open loop tests were correlated with closed loop tracking task results to evaluate those handling qualities related factors which affect the desirability of a depressed roll axis for air-to-air tracking.

TEST METHODS

In general, standard USAF Test Pilot School Flight Test Techniques (FTT's) were used to determine the lateral-directional characteristics of the DIGITAC aircraft (Ref. 11). All tests were initiated from a trimmed condition at 15,000 feet pressure altitude and 350 KIAS. These FTT's are summarized below.

1. Dutch Roll. A rudder doublet was used to excite the Dutch roll modes of the aircraft for the various flight control configurations. In addition, aileron doublets were performed to determine if the Dutch roll was excited by aileron inputs.

2. Spiral Mode. The aircraft was placed in a stabilized 20 degree bank turn. At test initiation, the stick was released and the time to either half or double amplitude measured.

31

3. Roll Mode. Aileron rolls were performed to determine the roll mode time constant. Step aileron inputs were used to measure roll perfomance. Roll perfomance was measured for both left and right rolls. Full deflection aileron rolls were initiated from level flight with the input held through 360 degrees of roll.

4. Frequency Response. Lateral frequency sweeps were used to determine the aircraft lateral frequency response. Sinusoidal aileron inputs were initated at a constant magnitude and frequency. The frequency was increased in steps to the maximum frequency obtainable by the pilot.

CLOSED LOOP OBJECTIVES

The closed loop testing objective was to evaluate the effect of depressing the roll axis on the air-to-air tracking task. To achieve this, each of the five depressed roll axes were evaluated several times by each pilot with a pilot-in-the-loop tracking task using a maneuvering T-38 airborne target. The task was designed to primarily excite the lateral-directional dynamics of the DIGITAC aircraft. The performance criteria were tracking within three mils of the aimpoint (intersection of T-38 tailpipes) for four consecutive seconds for desired performance and one second for adequate performance. This criteria was established to create a high gain tracking task which should

32

provide better differentiation between the roll axes.

For the first 15 seconds of each tracking task, the T-38 target flew a level 3 g, left turn. During this interval, the DIGITAC pilot moved the pipper from an initial 50 mil lateral offset and attempted to precisely track (fine track) the T-38. After the 15 second interval, the T-38 initiated one of two maneuvers to cause the DIGITAC pilot to further excite the lateral axis while continuing to track (maneuver track). The two maneuvers were a loaded S turn on the horizon and a loaded half barrel roll (reversal). The S turn provided changes in target roll direction. The reversal provided a constantly varying target bank angle. The pilot was not told which depression was being evaluated nor which of the two maneuvers the target would fly. This was done to prevent any bias in the evaluation of that roll axis depression.

At the completion of the maneuvering, the DIGITAC pilot assessed the compensation, workload and performance, then gave separate Cooper-Harper ratings to the fine tracking and maneuvering portions (Ref. 12). The Cooper-Harper rating scale is shown in Figure 8. Comments were made and recorded both during and immediately after each manueuver. Comments especially elicited were those concerning predictibility (pipper position vs control input), performance, and compensation required to achieve tracking.
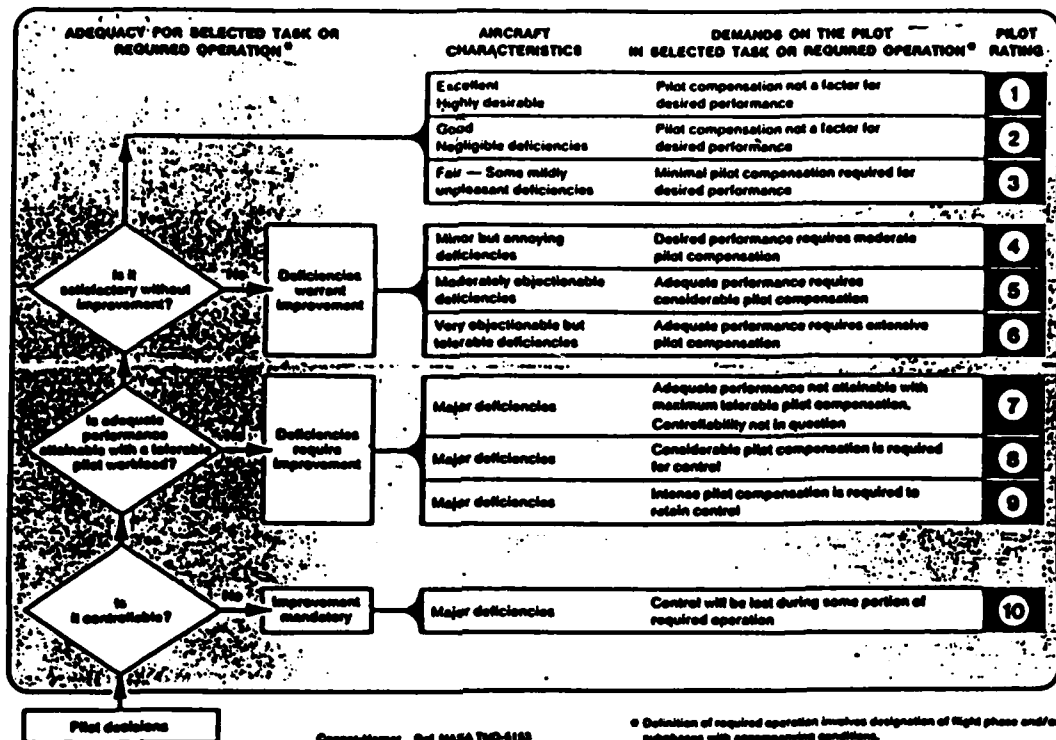
DEFINITIONS FROM TN-D-5153

COMPENSATION

The measure of additional pilot effort and attention required to maintain a given level of performance in the face of deficient vehicle characteristics.

HANDLING QUALITIES

Those qualities or characteristics of an aircraft that govern the ease and precision with which a pilot is able to perform the tasks required in support of an aircraft role.

MISSION

The composite of pilot-vehicle functions that must be performed to fulfill operational requirements. May be specified for a role, complete flight, flight phase, or flight subphase.

PERFORMANCE

The precision of control with respect to aircraft movement that a pilot is able to achieve in performing a task. (Pilot-vehicle performance is a measure of handling performance. Pilot performance is a measure of the manner or efficiency with which a pilot moves the principal controls in performing a task.)

ROLE

The function or purpose that defines the primary use of an aircraft.

TASK

The actual work assigned a pilot to be performed in completion of or as representative of a designated flight segment.

WORKLOAD

The integrated physical and mental effort required to perform a specified piloting task.

FIGURE 8: COOPER-HARPER RATING SCALE

DATA REDUCTION AND TEST RESULTS

OPEN LOOP RESULTS

Data were reduced from telemetry ground station time histories of the test aircraft parameters. Dutch roll characteristics were determined from the rudder position and angle of sideslip traces. The spiral characteristics were determined from cockpit instrumention values of bank angle and time. The roll mode time constants were derived from time histories of roll rate. The frequency response of the DIGITAC aircraft was determined from time histories of lateral stick force as the input and roll rate response as the output (Ref. 13).

The results of the open loop tests were tabulated for validation of the analytical aircraft model. The dutch roll was heavily damped and the spiral mode nearly neutrally stable for the CAS and multimode control systems as expected. In addition, specific test parameters were compared to determine any trends which might occur as a result of depressing the aircraft roll axis. The parameters selected for analysis were those which would impact the handling qualities and performance of a depressed roll axis aircraft for the air-to-air tracking task. These were:

1. Roll Mode Time Constant. Of primary concern to the pilot during the air-to-air tracking task is the time required for the

35

aircraft to reach a steady state roll rate in response to a lateral stick input. The roll performance parameter useful in describing the roll response of an aircraft is the roll mode time constant. Physically, it is the time for the aircraft to reach 63% of its steady-state roll rate following a step aileron input. The roll mode time constant directly influences pilot opinion of the maneuvering capability of an aircraft.

The effect of depressing the roll axis on the roll mode time constant is shown in Figure 9. The roll mode time constant decreases as augmentation is added to the basic mechanical flight control system. An increase in roll response, evidenced by a decrease in $\mathcal{T}_R$, is observed with the control augmentation system on. This is due in part, to the additional aileron input from that system as shown in Figure 10. The increase in roll response is also due to a rudder input from a CAS aileron to rudder interconnect. As the roll axis is depressed with the Multimode system, the roll mode time constant continues to decrease as a result of increasing rudder commands used to effectively depress the roll axis. Pilot performance in the air-to-air tracking task should increase as a result of this increased roll response.

2. Steady-State Roll Rate. The steady-state roll rate of the aircraft was shown to be essentially constant for all roll axis depressions. This result was expected due to roll rate limiting factors present in the flight control system.

YA-7D USAF S/N 67-14583
CRUISE CONFIGURATION - CG 29% MAC
15,000 FEET PA - 350 KIAS
FLIGHT TEST DATA (22 APR-17 MAY 1983)
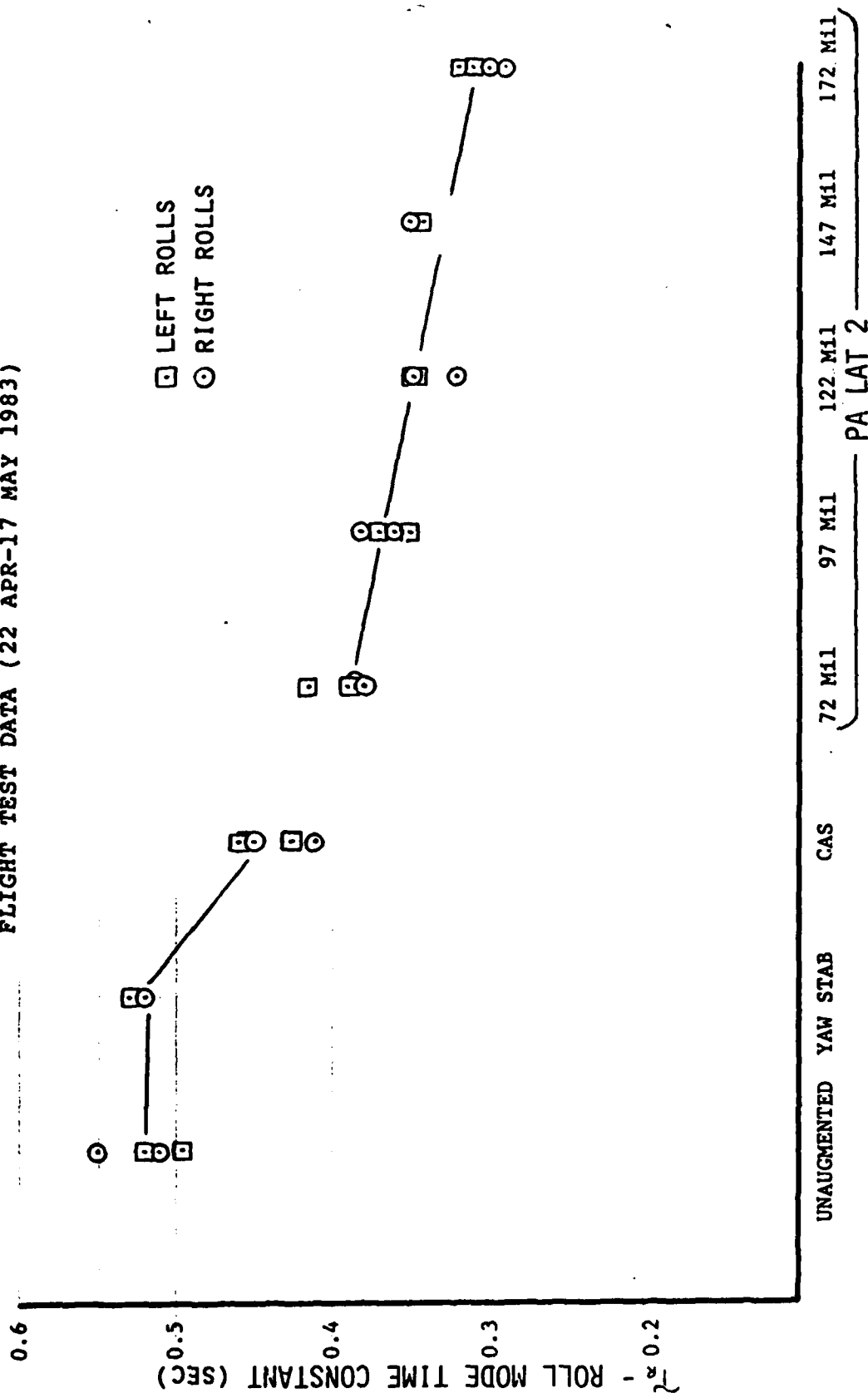
□ LEFT ROLLS
⊙ RIGHT ROLLS

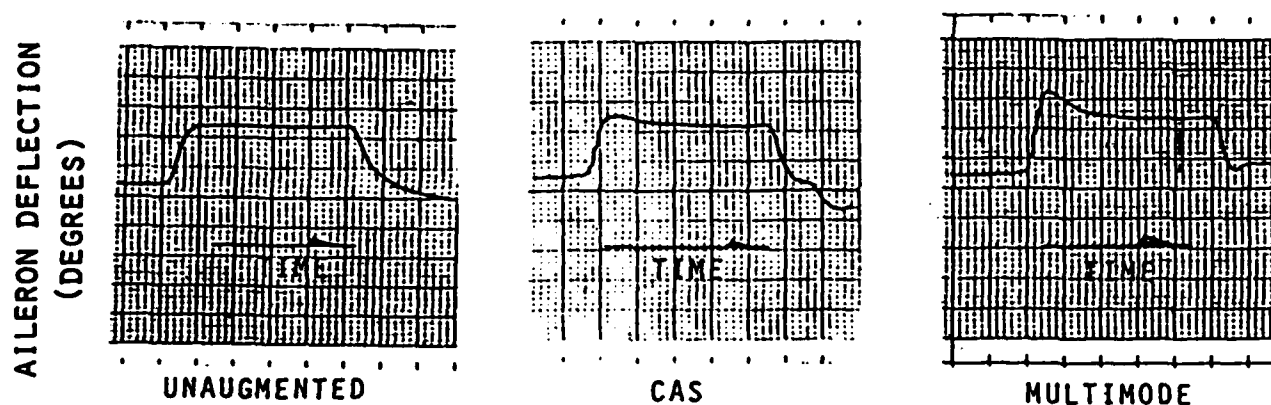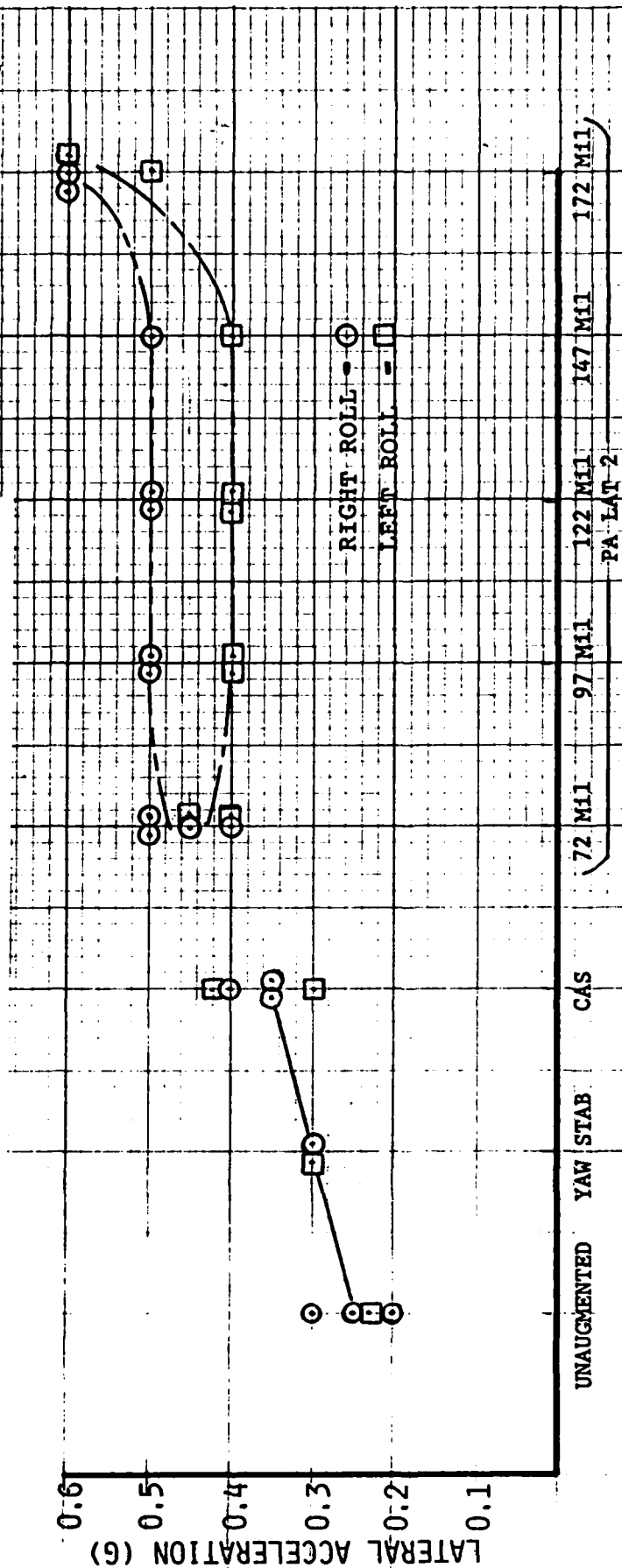FIGURE 9: ROLL MODE TIME CONSTANT VS CONTROL SYSTEM CONFIGURATION

FIGURE 10:   AILERON DEFLECTION COMPARISON FOR STEP AILERON INPUT

3.   Steady-State Yaw Rate.   The yaw rate occurring during
roll maneuvers increased with roll axis depression.   This was due
to larger rudder inputs from the Multimode system increasing roll
axis depression.

4.   Lateral Acceleration.   The change in lateral
acceleration experienced by the pilot in rolling maneuvers is
shown in Figure 11.   This figure indicates an increase in lateral
acceleration for rolling maneuvers with the Multimodes engaged
over the basic aircraft control system.   The lateral
acceleration, however, appears to remain relatively constant for
the first four roll axis depressions.   A increase in lateral
acceleration is noted for the 172 mil depression setting.   This

38

YA-7D USAF S/N 67-14583
CRUISE CONFIGURATION - CG 29% MAC
15,000 FEET PA - 350 KIAS
FLIGHT TEST DATA (22 APR-17 MAY 1983)

RIGHT ROLL - ⊙
LEFT ROLL - ⊡

| UNAUGMENTED | YAW STAB | CAS | 72 M11 | 97 M11 | 122 M11 | 147 M11 | 172 M11 |
| | | | | | PA LAT-2 | | |

CONTROL SYSTEM CONFIGURATION

LATERAL ACCELERATION (G)

FIGURE 1. LATERAL ACCELERATION VS CONTROL SYSTEM CONFIGURATION

39

increase may impact pilot rating as a function pilot comfort. The difference between left and right rolls is probably ªue to the instrumentation pod (asymmetric store) on the right wing.

CLOSED LOOP RESULTS

Figures 12 through 14 depict Cooper-Harper ratings given by all project pilots for different roll axis depressions. These ratings are separated for the fine tracking and maueuvering tracking tasks. Each pilot flew each configuration at least twice during the test.

From Figure 12 for fine tracking, we note an obvious tendency for better ratings toward the 122 and 147 mil roll axis depressions. Similiar results were indicated for maneuvering tracking as shown in Figures 13 and 14.

It is interesting to note that overall for the fine tracking, the ratings are better than those for the maneuvering tracking. Pilots found it was more difficult to track the T-38 during the "S" turn and reversal than through the level 3 g turn fine tracking.

Pilot comments showed definite trends. The comments clearly showed pilot dislike for the 72 mil roll axis depression. There was not a single favorable comment for this axis. Although the 72 mil roll axis depression is close to what the pilots fly with operationally, they found that the more depressed roll axes did not produce as much sight oscillation and therefore made lateral

YA-7D USAF S/N 67-14583 , TF41-A-1 ENGINE

CRUISE CONFIGURATION , INSTRUMENTATION POD ON STATION 6

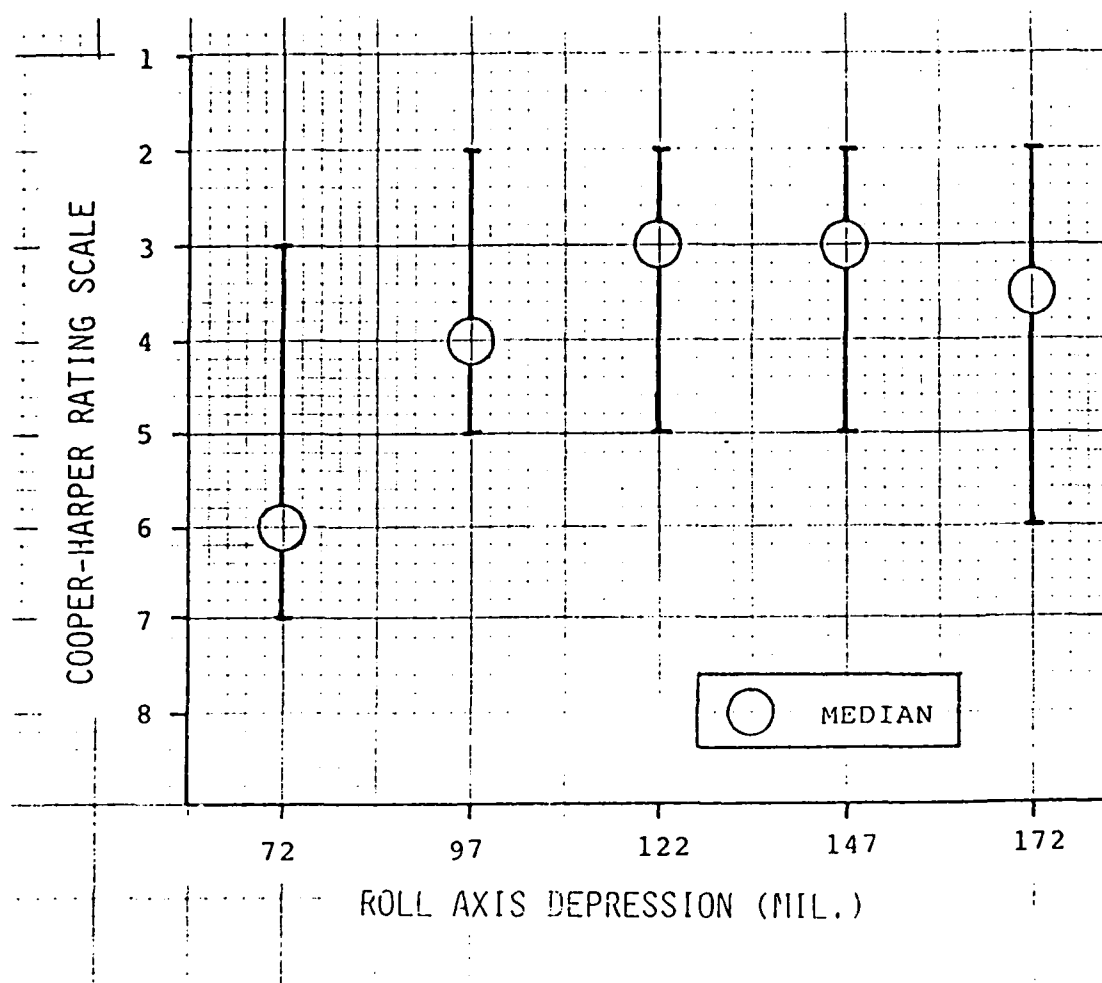15000 FEET PA , 350 KIAS , RANGE 1500 FEET

FIGURE 12:   COOPER-HARPER RATINGS BY ALL PILOTS
FOR "FINE TRACKING"

YA-7D USAF S/N 67-14583 , TF41-A-1 ENGINE

CRUISE CONFIGURATION , INSTRUMENTATION POD ON STATION 6

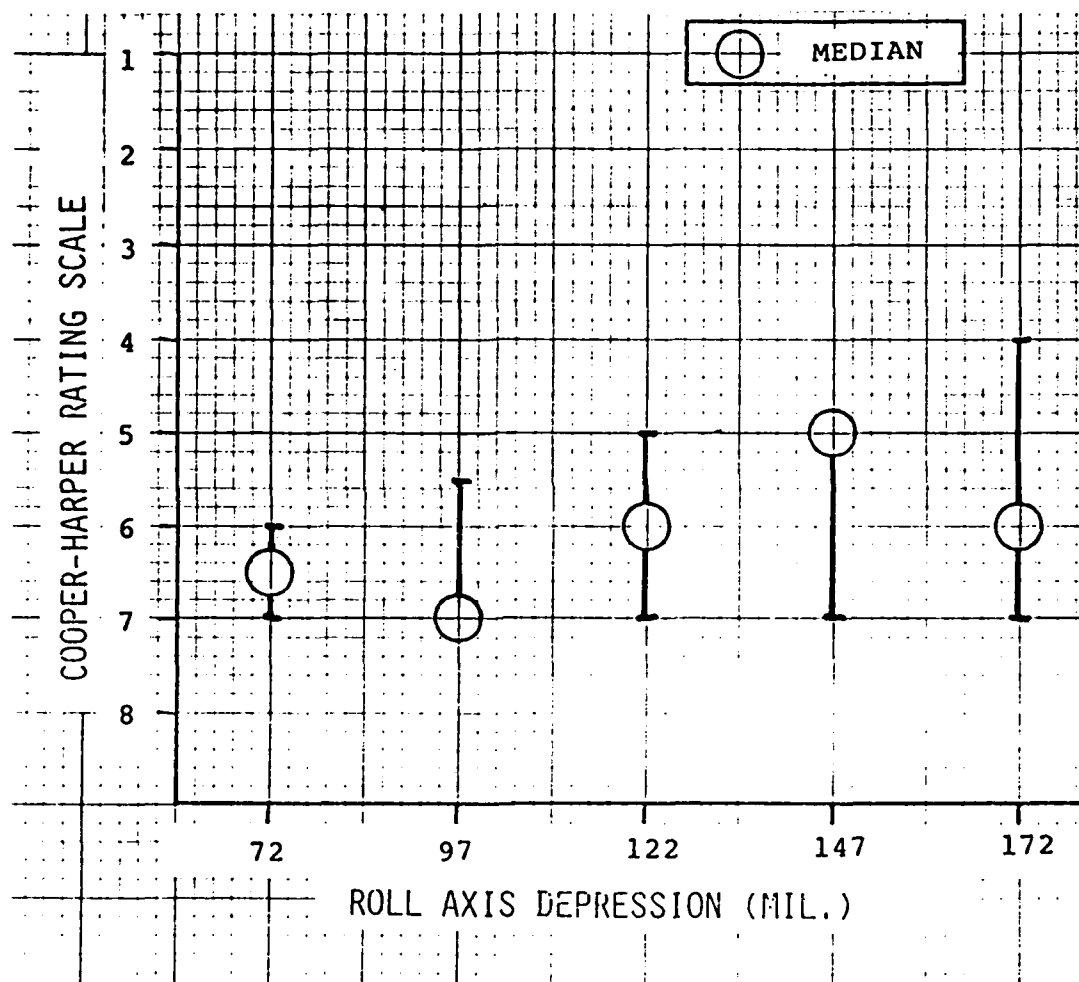15000 FEET PA , 350 KIAS , RANGE 1500 FEET

FIGURE 13:   COOPER-HARPER RATINGS BY ALL PILOTS
FOR MANEUVER TRACKING - "S TURN"

YA-7D USAF S/N 67-14583 , TF41-A-1 ENGINE

CRUISE CONFIGURATION , INSTRUMENTATION POD ON STATION 6

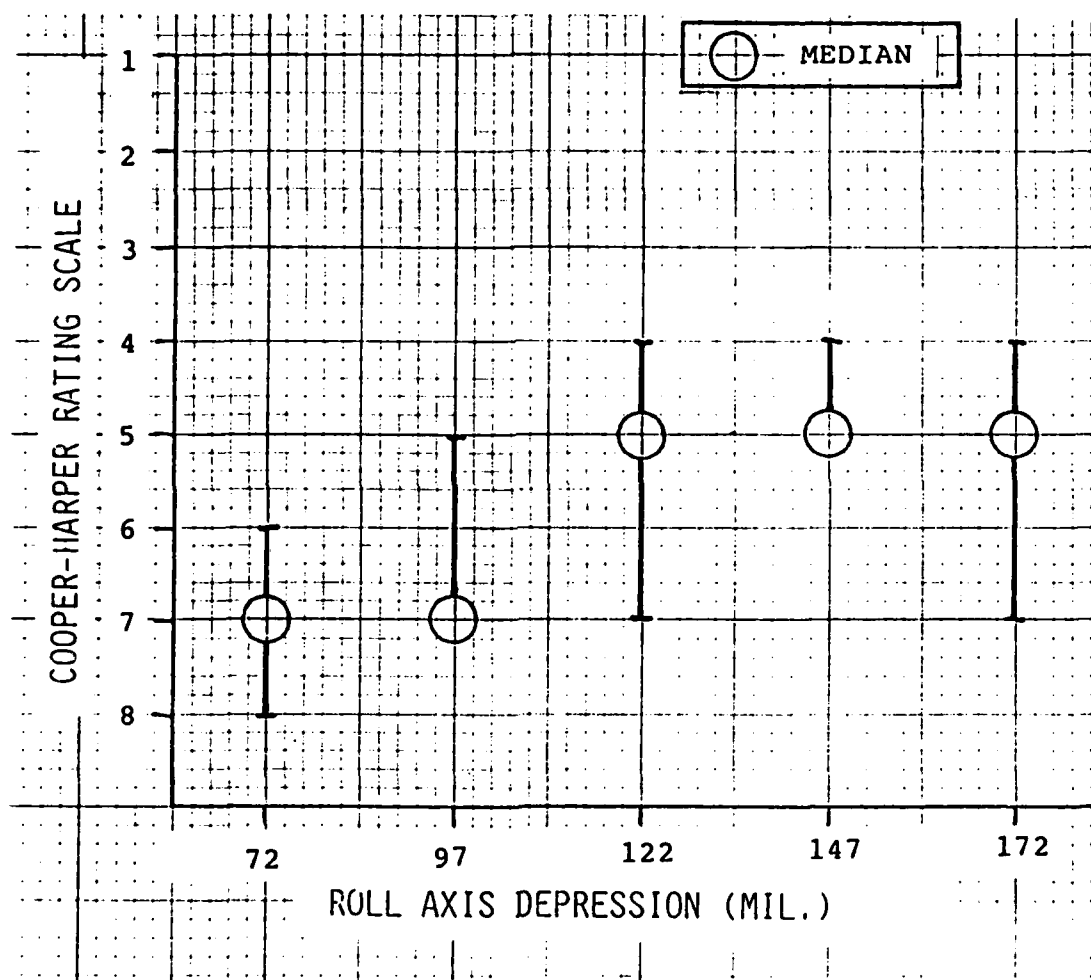15000 FEET PA , 350 KIAS , RANGE 1500 FEET

FIGURE 14:   COOPER-HARPER RATINGS BY ALL PILOTS
              FOR MANEUVER TRACKING - "REVERSAL"

tracking easier. The amount of favorable comments increased as the roll axis depression increased up to and including 147 mils. Comments for the 172 mil depression were all distinctly less favorable than for the 147 mil depression. Pilots felt the lateral response was too quick, which tended to produce lateral oscillations. Selected comments typical for the roll axis depressions are listed in Table 5.

There were some notable lessons learned during these pilot-in the-loop evaluations. One was that the performance criteria should reflect only changes in the independent variable: project pilots felt that some of the Cooper-Harper ratings were artificially lowered by errors in the longitudinal axis when only lateral axis changes were being evaluated. Another was that control harmony (pipper movement vs control deflection) changed for the longitudinal and lateral axes for some roll axis depressions. This caused problems with pipper predictability. Roll axis depression preference might well be different depending on where this harmony occurs.

TYPICAL PILOT COMMENTS BY ROLL AXIS DEPRESSION

72 MILS

Anywhere but on him

Not predictable in performance

Lateral oscillations with aggressiveness

97 MILS

Smooth inputs help

Borderline predictability

Some lateral oscillations

122 MILS

Lateral control pretty good

Almost no lateral oscillations

Never got off of fuselage and wings

147 MILS

Good predictability - very stable

Easy to control and predict

Good predictability and responsiveness

172 MILS

Some tendancy to overcontrol

Lateral oscillations

Lateral predictability is a problem

TABLE V: TYPICAL PILOT COMMENTS FOR ALL TRACKING TASKS

V. COMPARISON OF MODEL AND FLIGHT TEST RESULTS

The analytical models were compared to flight test results for aileron rolls and frequency sweeps. The nonlinear model was used to generate time histories of a full stick deflection step aileron input. Roll rate and yaw rate were the primary time histories used for comparison with flight test time histories. There was good correlation between flight test and model results for the CAS as shown in Figure 15. A mechanical system only comparison also showed good agreement (Figure 16). This level of agreement for both roll and yaw rate time histories indicate that the nonlinear models of the mechanical and CAS control systems, along with the airframe, closely approximate the actual aircraft. The yaw rate match could probably be improved by modifying the lateral-directional cross stability derivatives, primarily C_{yp} or $C_{n\delta a}$.

A check of the roll rate to lateral stick force frequency response against a frequency response plot generated from the linearized roll CAS model shows good agreement as shown in Figure 17. The roll CAS model was a ninth order linearized CAS and mechanical roll flight control system and lateral-directional aircraft dynamics model (Appendix D). It did not include the rudder flight control system nor the lateral relative kinematics. It should be noted that the flight test frequency response characteristics were hand reduced hence limiting the number of discrete points and thus preventing the drawing of a flight test frequency response curve. A frequency response analysis program

46
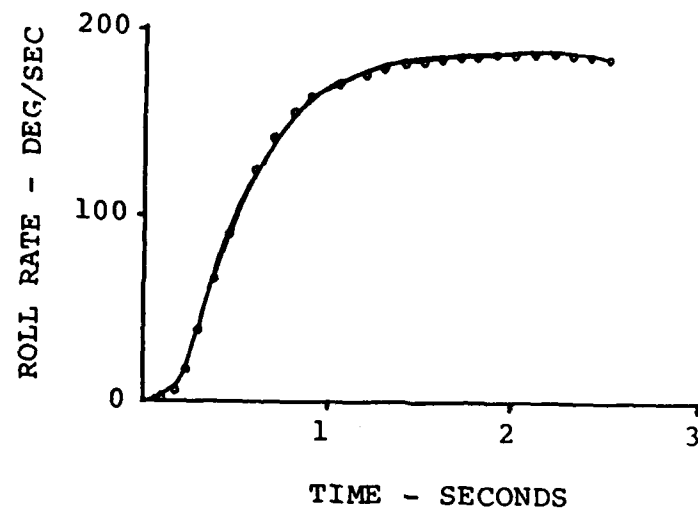
— Flight Test

∘ Nonlinear Model

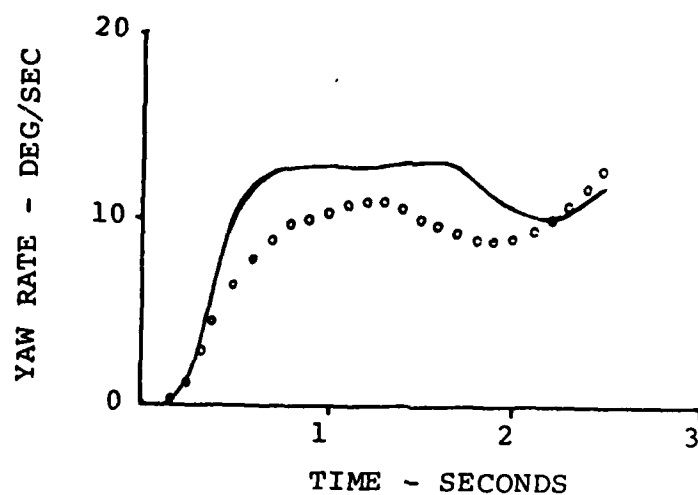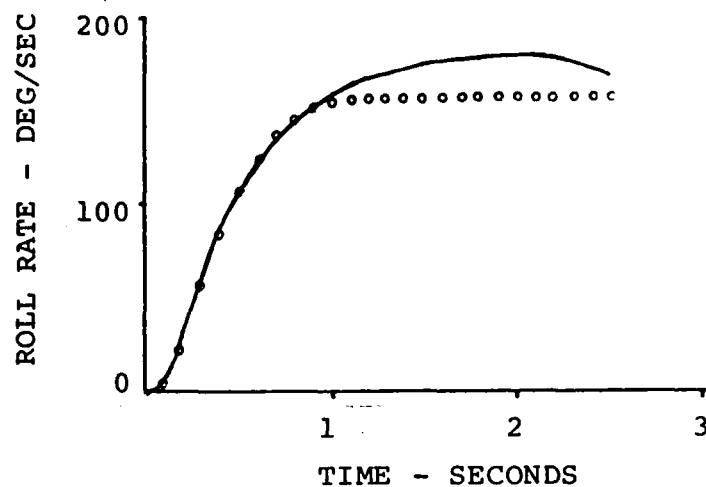FIGURE 15: MODEL AND FLIGHT TEST DATA COMPARISON OF ROLL AND YAW
RATES FOR STEP AILERON INPUT - MECHANICAL AND CAS

47

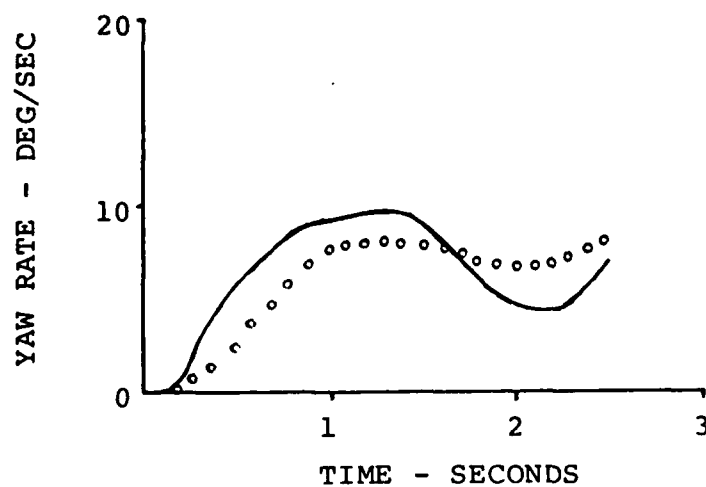FIGURE 16: MODEL AND FLIGHT TEST DATA COMPARISON OF ROLL AND YAW
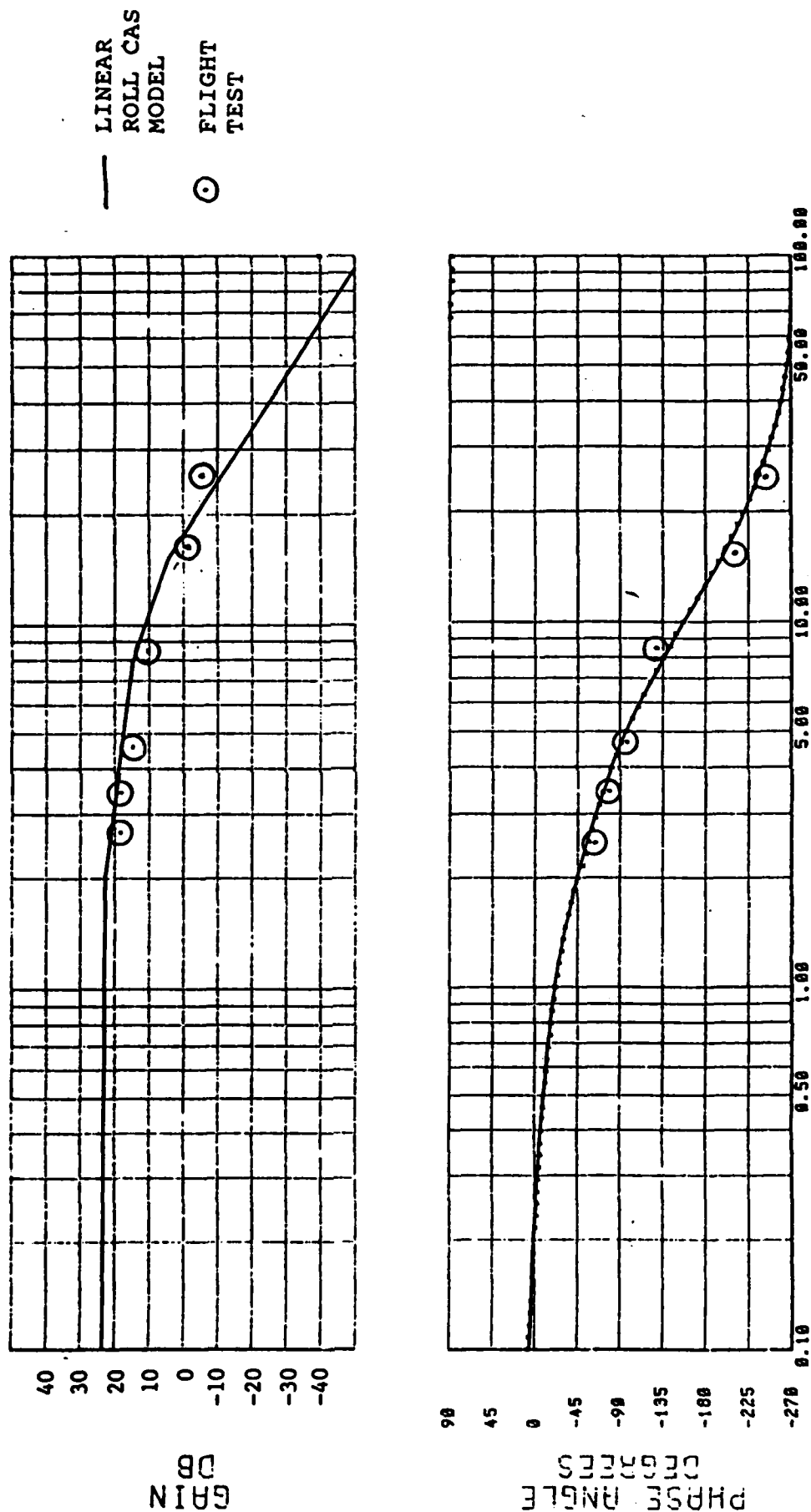RATES FOR STEP AILERON INPUT - MECHANICAL ONLY

FIGURE 17: COMPARISON OF MODEL AND FLIGHT TEST FREQUENCY RESPONSE DATA

49

was available but could not be used because the DIGITAC data was not in the proper format.

There were two differences between flight test and model derived results. First there was an asymmetrically loaded instrumentation pod on the right wing which means the X and Z axes are not exactly in the plane of symmetry. This could account for some of the differences between flight test and model data. The second difference was that the stability derivatives used in the nonlinear simulation and linear model correspond to Mach = 0.60 while the flight testing was done at Mach = 0.68. However, the difference in dynamic pressure is accounted for since stability derivatives were used in the nonlinear model. Checks of stability derivative variation with the difference in Mach numbers (0.6 to 0.68) showed negligible changes.

The results achieved during closed loop testing, generally agree with the results predicted by the preliminary linear analysis. Pilot comments indicated that the system damping increased as the roll axis depression increased. Pilot compensation (pilot lead required), as shown by the Cooper-Harper ratings, decreased as the roll axis depression increased. The results obtained at the most depressed axis, 172 mils, differed significantly from what was expected. The expected results were a further decrease in pilot compensation required, and an increase in system damping. The results obtained in closed loop tracking tests indicated that more pilot compensation was required and that the system damping decreased resulting in lateral oscillations. This indicates the possible existence of

50

an optimum operating point or region on the root locus. This could also be an indication that other factors, such as the increase in lateral acceleration, are having a significant impact on aircraft lateral-directional handling qualities.

VI. CONCLUSIONS

The thesis objective of developing an analytical model of the air-to-air tracking task and comparing it to flight test was accomplished. A nonlinear simulation and a linear model of the air-to-air tracking task were developed. A comparison of the nonlinear simulation roll and yaw time histories for a step aileron input, against flight test data, showed good agreement. A linearized roll model did show good agreement with flight test data with respect to frequency response for roll rate to lateral stick force. However, model size limitations of the linear analysis program prevented the accurate linear modelling of the air-to-air tracking task.

The results achieved during open loop testing characterized the effect of depressing the roll axis on the lateral-directional dynamics. The most noticeable change is the reduction in roll mode time constant as the roll axis gets further depressed. The closed loop handling qualities evaluation determined that the 122 and 147 mil roll axis depressions were the optimum for the air-to-air tracking tests. These results are valid for test conditions of 350 KIAS, 15,000 feet PA with a 3g target at 1,500 feet range and with a fixed depressed sight.

RECOMMENDATIONS

1. Additional work should be done on the nonlinear model. The multimode control system should be incorporated and the

tracking loop should be closed with the addition of a pilot
model.

2. Further linear analysis should be done to incorporate the
flight control system effects. The investigation into the
effects of depressing the aircraft roll axis should be continued.

3. The flight test data reduction procedure for the DIGITAC
aircraft needs to be modified to allow the use of computer
routines for frequency response analysis.

REFERENCES

1. Damman, Lawrence M., Capt, USAF, AFFTC-TR-76-15 Flight Test Development and Evaluation of a Multimode Digital Flight Control System Implemented in an A-7D (DIGITAC), AFFTC, Edwards AFB, CA, June 1976.

2. Clarke, Robert, AFFDL-TR-75-97 Flight Test Evaluation of a Digital Multimode Flight Control System for the A-7D Aircraft, Air Force Flight Dynamics Laboratory, Wright Patterson AFB, OH, November 1975.

3. Lipari, Louis J., AFFTC-TR-79-5 DIGITAC II Phase 1, Yaw Control Laws and Redundancy Evaluation, AFFTC, Edwards AFB, CA, May 1979.

4. Anhalt, David A., Capt, USAF, et al., A-7D DIGITAC Limited Air-to-Air Tracking Evaluation Using a Depressible Roll Axis - Letter Report, USAF Test Pilot School, AFFTC, Class 81A, Edwards AFB, CA, November 1981.

5. McClendon, Mike H., Capt, USAF, et al., YA-7D DIGITAC Limited Air-to-Air Tracking Evaluation Using a Dynamically Varying Roll Axis - Letter Report, USAF Test Pilot School, AFFTC, Class 82A, Edwards AFB, CA, October 1983.

6. Jeske, R.A., et al., Final Engineering Report Automatic Flight Control System For A-7D/E Aircraft, Report No.2-53560/9R-5448, LTV Aerospace Corporation, Undated.

7. Roskam, Jan., Airplane Flight Dynamics and Automatic Flight Controls, Part I, Roskam Aviation and Engineering Corporation, Lawerence, KS, 1979.

8. Clarke, Robert, AFFDL-TR-76-121 A-7D Digital Multimode Flight Control System Flight Test and Weapon Delivery Evaluation, Air Force Flight Dynamics Laboratory, Wright-Patterson AFB, OH, December 1976.

9. Larimar, S.J., TOTAL - An Interactive Computer Aided Design Program for Digital and Continuous Control System Analysis and Synthesis. Master's Thesis, Air Force Institute of Technology, Wright-Patterson AFB, OH, March 1978.

10. Eischens, William L., Capt, USAF, et al., Evaluation of an Analytical Model of the Air-to-Air Tracking Task - Letter Report, USAF Test Pilot School, AFFTC, Class 82B, Edwards AFB, CA, June 1983.

11. Flying Qualities Theory and Flight Test Techniques, Chapter 7, Dynamics, USAF Test Pilot School, AFFTC, Edwards AFB, CA, July 1981.

12. Cooper, G.E., and Harper, R.D.,Jr, <u>The Use of Pilot Ratings in the Evaluation of Aircraft Handling Qualities</u>, NASA TN-D-5153, April 1969.

13. Hall, G.W., <u>A Collection of Flight Test Data Reduction Techniques</u>, Calspan FRM No. 177, June 1973.

14. <u>T.O. 1A-7D-1 Flight Manual</u>, 1 February 1979, Change 9, 1 April 1982, T.O 1A-7D-1S-136, 19 November 1982.

15. <u>YA-7D S/N 67-14583 Partial Flight Manual</u>, AFFTC, Edwards AFB, CA, 15 February 1979, Change 2, 7 April 1980.

16. D'Azzo, J.J. And Houpis, C.H., <u>Linear Control System Analysis and Design</u>. McGraw Hill Book Company, 1981.

17. McRuer, D., Ashkenas, I., and Graham, D., <u>Aircraft Dynamics and Automatic Control</u>, Princeton University Press, 1973.

18. Eischens, William L., Capt, USAF, <u>et al.</u>, <u>Air-to-Air Tracking Evaluation of the YA-7D DIGITAC Aircraft - Test Plan</u>, USAF Test Pilot School, AFFTC, Class 82B, Edwards AFB, CA, April 1983.

APPENDIX   A

DESCRIPTION OF FLIGHT CONTROLS

DESCRIPTION OF FLIGHT CONTROLS

FLIGHT CONTROLS

The standard A-7D flight control system includes a control
augmentation system (CAS) implemented by feeding stick and rudder
pedal forces into an analog computer. This CAS is in addition to
a mechanical path that physically links the primary control
surface actuators to the stick in each axis. Dual electro-
hydraulic actuators connected in series with the primary mech-
anical linkage implement pilot inputs with additional partial
control authority. All control surfaces are fully powered by
irreversible dual tandem hydraulic actuators. Control surfaces
are an all moving horizontal tail for longitudinal control, a
conventional rudder for directional control, and a combination of
ailerons and spoiler/deflectors for roll control. Analog com-
puters in the standard AFCS were removed and replaced with the
multimode (DFCS) for DIGITAC testing (3:179).

MECHANICAL FLIGHT CONTROL SYSTEM

The primary mechanical flight control system remains
unchanged by installation of the DFCS. Conventional control rods
link the pilot's center stick controller to control surface
actuators in both longitudinal and lateral axes. Cables link the
rudder pedals to actuators in the directional axis. Two
independent hydraulic systems power the control surface actuators

57

during normal operation. The longitudinal feel system consists
of a dual gradient feel spring, two bob weights, and two viscous
dampers. These dual bob weights produce a static force gradient
proportional to normal acceleration in addition to the feel
spring force gradient. The dual bob weights also produce dynamic
forces proportional to pitch acceleration. With viscous damping,
this system minimizes the possibility of pilot induced
oscillations. The longitudinal trim system is a parallel pulse
type using an actuator in parallel with a dual rate feel spring.
Lateral stick feel is obtained with a simple linear spring and
viscous damper. A feel isolation actuator in the lateral linkage
prevents feedback from the spoiler/deflector breakout device.
Directional feel is obtained from linear springs which produce
different force gradients in clean and landing configurations.
Directional axis trim uses the standard flight control system
actuator.

MULTIMODE DIGITAL FLIGHT CONTROL SYSTEM

General:

The DFCS is a dual channel, three-axis system using whole word
computer techniques. It provides inner loop stability and con-
trol augmentation functions and outer loop automatic pilot relief
functions. The DFCS was designed not only to duplicate the
operation and functions of the standard A-7D AFCS (described in
chapter II), but also to provide pilot selectable control modes

(multimodes) which implement optimized control laws for improved
aircraft operational performance. These operational modes
essentially provide improved control of either aircraft
flightpath or aircraft attitude depending on the mode selected.
Multimodes are called Pitch and Lateral Flightpath (FP), and
Pitch and Lateral Precision Attitude (PA). Standard A-7D AFCS
modes are selected on the standard AFCS control
panel which has been rewired, while multimodes are selected from
a new multimode control panel in combination with the standard
AFCS control panel. The DFCS uses existing A-7D AFCS sensors and
actuators in addition to sensors added for multimode features and
for dual redundancy. DFCS hardware consists of the following:

1. Two central processor units (CPU's) with Honeywell
   HDC-301 processors.

2. Two SEMS-8 memory units (8k each).

3. A multimode control and display panel which provides
   engage/disengage switches for multimode
   functions, engage/status switches for CPU's, and
   gain change capability through seven three-position
   switches.

4. Two remote terminals providing interface and signal conditioning for both aircraft sensors and discrete switching. These terminals also provide interface with the multiplex data bus by wire or fiber optics.

5. Dual rudder linkage position transducers and a second lateral accelerometer.

6. Dual aileron position transducers.

CPU's, memory units, and interface units are located in the left avionics bay while the multimode control panel is mounted in the cockpit on the left outboard console.

In addition to the normal A-7D sensor inputs, the DFCS uses airspeed and altitude inputs from the air data computer, angle of attack (AOA) information from the AOA vane on the flight test nose boom, and attitude information from the ASN-50 attitude reference system. The noseboom AOA vane is the primary source of AOA for multimode control law computations. For safety reasons, the boom vane transducer is powered from the DFCS rather than the flight test instrumentation power supply. Connection of the boom AOA transducer to flight test instrumentation is made from the DFCS interface unit through an isolation resistor. This configuration ensures isolation of the boom AOA signal from flight test instrumentation and through comparison monitoring provides a safe flight control input.

Standard A-7D AFCS Modes:

Control modes provided by the DFCS include standard A-7D
AFCS modes of:

1. Yaw stabilization

2. Pitch and roll control augmentation

3. Attitude hold

4. Heading hold

5. Heading select

6. Altitude hold

Performance and function of each of these modes is the same as
described in the A-7D Flight Manual (14:1-91).

DFCS Optimized Control Laws:

Stick-force-per-g gradient for both FP and PA modes is
designed to match the midpoint of the normal A-7D gradient. In
FP and PA mode, the roll and pitch stick force shaping is a
parabolic function which eliminats the dead band, produces quick-
er stick command response to initial inputs and provides smooth
control at small input levels. Gain scheduling varies feedback
gains as a function of dynamic pressure in both roll and yaw
axes. The yaw axis uses kinematically derived sideslip rate,
measured lateral acceleration and pedal position as inputs in

lieu of an aileron-to-rudder interconnect. This provides improved coordination and minimizes sideslip due to gusts. The derived signal is supplied to the rudder through a lag-lead shaping network to enhance directional stability at high AOA. Dynamic pressure scheduled gain compensates for varying rudder effectiveness.

Flightpath Mode:

The FP mode provides optimized flightpath response for large amplitude combat maneuvers which are typical in air-to-ground bombing or air combat maneuvering. Stick force sensors are used for both pitch and roll inputs, and rudder pedal position sensors are used for yaw inputs. FP mode provides rapid normal acceleration response at the expense of increased pitch rate overshoot and rapid roll rate response. FP mode also includes a pseudo-neutral speed stability which decreases stick force required to maintain trim with speed changes.

Precision Attitude Mode:

The PA mode provides optimized attitude response for small amplitude fuselage pointing tasks which are typical in air-to-air and air-to-ground gunnery. As in FP mode, stick force sensors are used for both pitch and roll inputs and rudder pedal position sensors are used for yaw inputs. PA mode provides optimized pitch rate response for small perturbations around trim. Gust

response is minimized at the expense of normal acceleration overshoots. Pseudoneutral speed stability is implemented as in FP mode. The PA mode in pitch has an automatic, smoothly blended reversion to FP mode type characteristics at normal acceleration perturbations above 0.25 g's. When this limit is exceeded, the system approximates FP response characteristics by feeding back normal acceleration. Roll axis control laws are identical to those of FP mode. The yaw axis uses kinematically derived side-slip rate, lateral acceleration, and rudder pedal position inputs as in the FP mode. However, in PA mode, a ±0.05 g dead band is inserted in the lateral acceleration feedback path to prevent the system from opposing initial lateral accelerations. This provides better turbulence response as yaw rate is sensed and damped, resulting in lower rates with less weathercocking. As in the FP mode, automatic rudder trim is provided, and dynamic pressure scheduled gains are used in both roll and yaw axes.

An additional lateral-directional submode is provided in PA mode. This second submode or "gun" mode (PA LAT 2) compromises conventional coordination in favor of a pilot selectable depressed roll axis as long as lateral accelerations are low. It makes the aircraft roll about the depressed roll axis rather than the flightpath for roll rates up to 0.4 radians per second. Should pilot commanded roll rate exceed this limit, the DFCS will limit control surface commanded roll rate to a maximum of that selected by the pilot on the multimode control panel or 0.4 radians per second, whichever is least.

Analytical diagrams of the multimode pitch, roll, and yaw
axis are shown in Figures A1, A2, and A3 respectively. Various
configurations are selected on the cockpit control panel shown in
Figure A4. A detailed description of the longitudinal, yaw, and
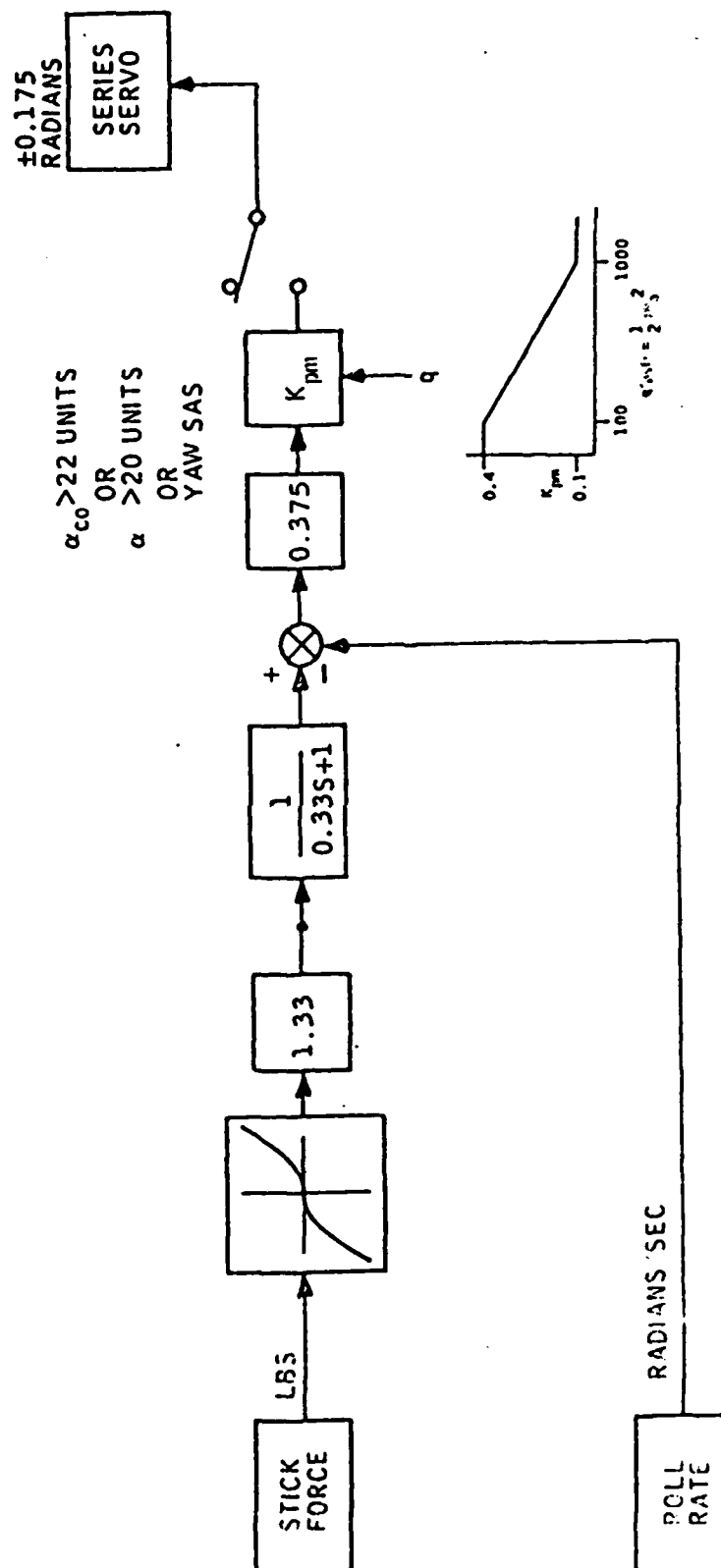roll axis is presented in Reference 3.

FIGURE A1: PA PITCH AXIS

65

FIGURE A2: PA ROLL AXIS

FIGURE A3: PA YAW AXIS

NOTE: K_{rm} is $\bar{q}$ scheduled gain
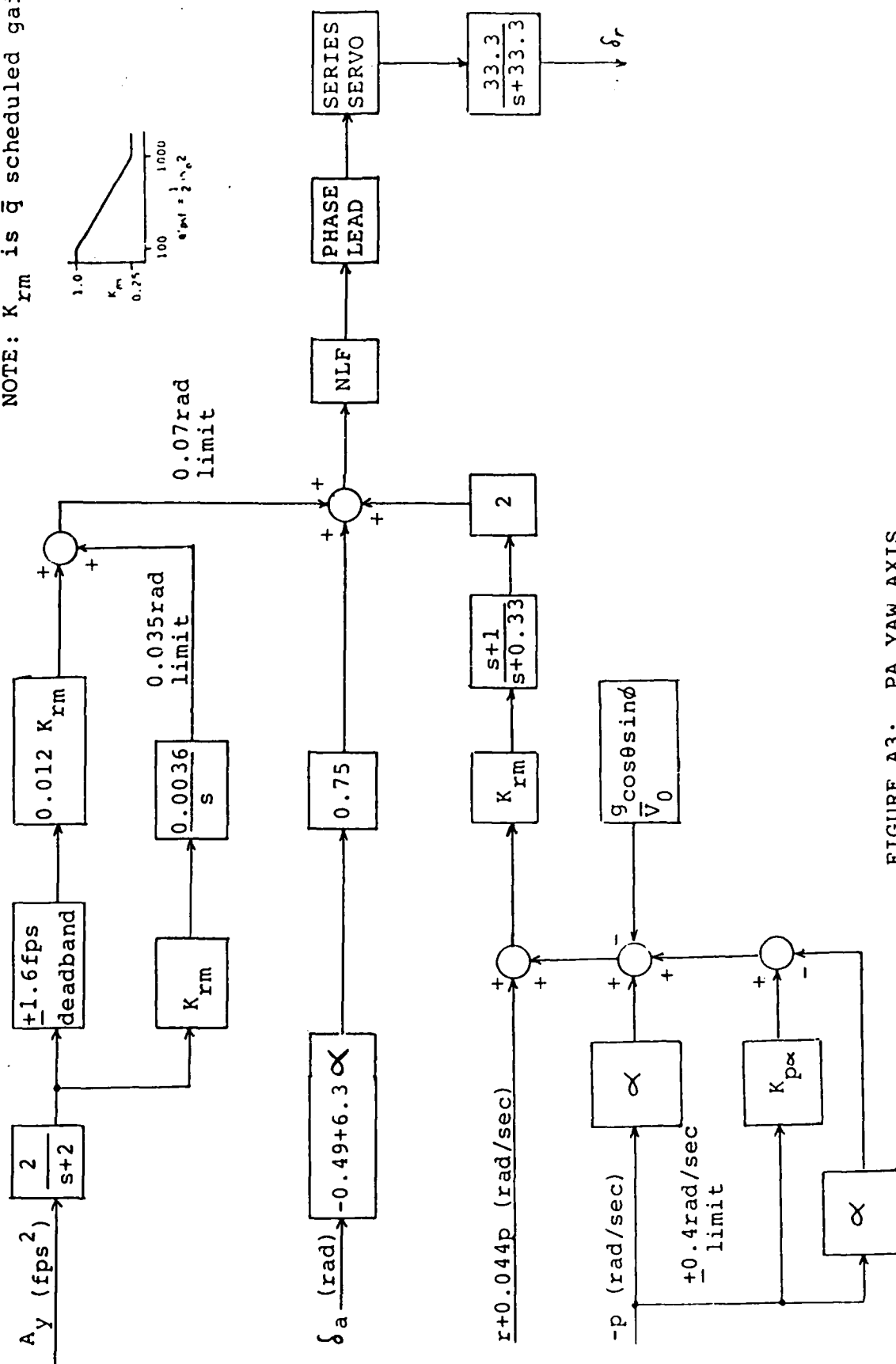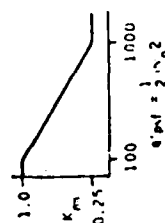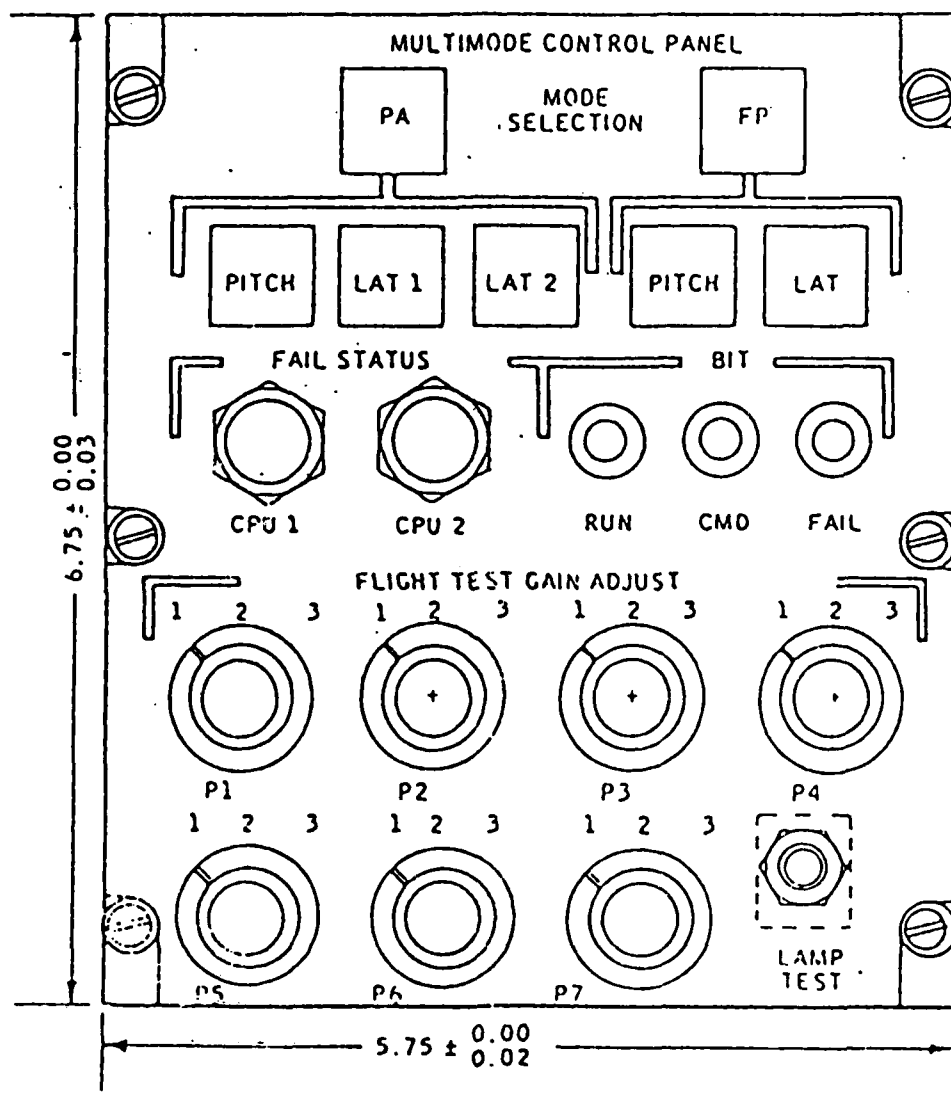
67

FIGURE A4: MULTIMODE CONTROL PANEL

YAW AXIS DESCRIPTION

Standard A-7D control systems are complemented in the yaw axis with a stability augmentation system (SAS). Yaw-rate feedback provides damping while an ARI and lateral acceleration feedback provide turn coordination (1:260).

In contrast, PA and FP modes provide a control augmentation system (CAS) with a command signal from rudder pedal position. A combination of lateral acceleration and yaw rate feedback provide damping and turn coordination (Figure A3). An ARI scheduled with AOA rather than the standard horizontal tail position was introduced for DIGITAC II testing. In the lateral acceleration loop, FP and PA modes are identical except for a ± 1.6 ft/sec^2 deadband in the proportional path of the PA mode. This path allows long term lateral trimming in both PA and FP modes, and improved lateral damping (weathercock stability) for large lateral accelerations. Lateral acceleration response differs from the standard SAS mode in that lateral acceleration response varies with dynamic pressure.

LAT 1:

To provide coordination in the conventional sense (zero sideslip), both FP and PA multimodes operate according to LAT 1 submode logic, unless LAT 2 is selected. The LAT 1 submode

control law comes directly from the following lateral force equation:

$$a_y = U_o (r_s + \dot{\hat{\beta}}) - g \sin \phi \cos \Theta$$

where: a_y = lateral acceleration at the cg

U_o = true airspeed along longitudinal axis

r_s = stability axis yaw rate

$\dot{\hat{\beta}}$ = sideslip rate relative to air mass

ϕ, Θ = roll and pitch attitude

If a_y is produced mainly by sideslip, maintaining zero sideslip rate would produce zero lateral acceleration. The criteria for $\dot{\hat{\beta}} = 0$ is satisfied by keeping control error small. Since yaw rate is measured in the body axis, stability axis yaw rate is obtained by resolving yaw rate (r) and roll rate (p) through AOA (α);

$$r_s = r \cos\alpha - p \sin\alpha$$

Assuming a small angle of attack;

$$r_s = r - p\alpha$$

And adding a small correction term because the yaw gyro has a 2.5 degree tilt;

$$r_s = r - p\alpha + .044p$$

Now assuming a_y is zero because β is small, and solving for $\dot{\beta}$;

$$\dot{\beta} = p\alpha - r - .044p + (g / V) \sin\phi \cos\theta$$

PA and FP multimode control laws implement this equation as shown in Figure A3. $\dot{\beta}$ is the control element and is kept small by driving the rudder with the highest loop gain possible. The multimode law of Figure A3 schedules K_{rm} with lead-lag shaping to give a higher gain without compromising stability margin (7:33).

LAT 2:

An additional PA submode adds a roll rate to rudder feedback signal to the $\dot{\beta}$ equation. LAT 2 control laws replace the $p\alpha$ term in the $\dot{\beta}$ equation with another term, $K_{p\alpha}$ (Figure A3). This $K_{p\alpha}$ term drives the rudder creating a new "critical yaw rate" which effectively alters the aircraft roll axis (7). Figure A5 illustrates the vector summation of body roll rate and roll rate induced body yaw rate to create a new, depressed roll axis. The amount of induced yaw rate from a given roll rate or roll rate to rudder gain, is a function of $K_{p\alpha}$ and P3 setting (Figure A3). A

71

deliberate stability yaw axis uncoordination is allowed in favor of altering roll axis orientation.

Note that there is a limit to the amount of uncoordination between roll axis and stability axis. When the limit of $\pm .4$ rad/sec (25 deg/sec) roll rate limit is reached, no further $K_{p\alpha}$ feed forward rudder command is generated. Additionally, $K_{p\alpha}$ is no longer cancelled, and the system attempts to constrain all further sideslip in the stability axis.

The P4 switch on the multimode control panel (Figure A4), sets $K_{p\alpha}$ and effectively selects reference roll axis. Switch P3 applies fixed gains of 1, 1.45, and 2 to the reference roll axis, which can further depress roll axis.

Table Al

Roll Rate To Rudder Gain

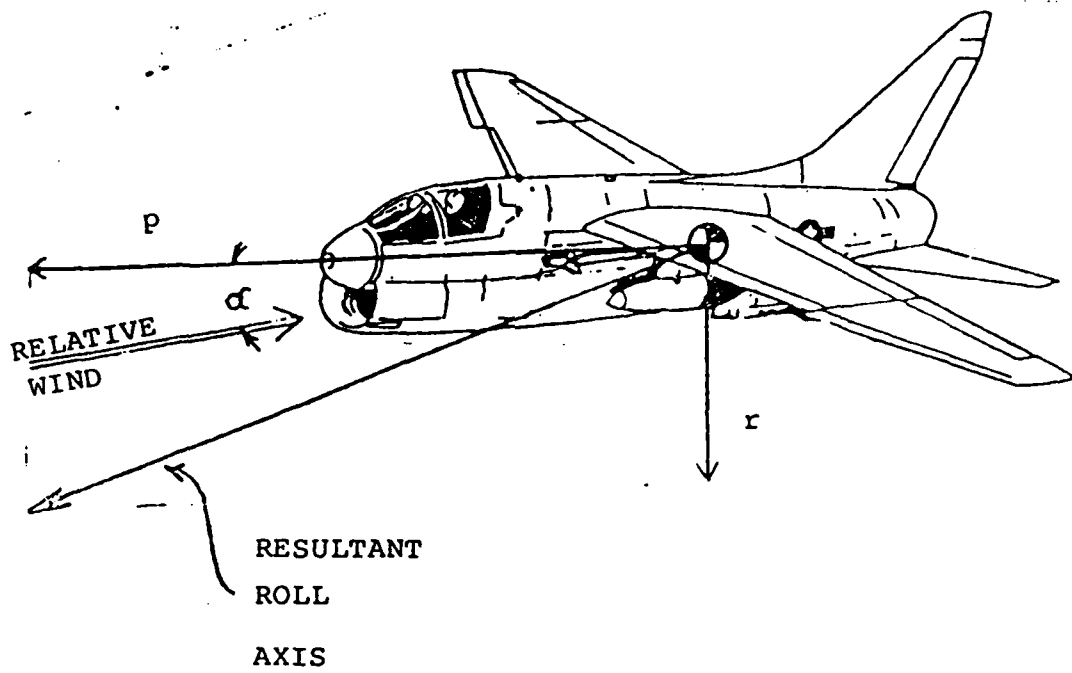| $K_{p\alpha}$	Reference Roll Axis Depression WRT Body Axis
0.072	72 mils
0.097	97 mils
0.122	122 mils
0.147	147 mils
0.172	172 mils

72

FIGURE A5: DEPRESSED ROLL AXIS ILLUSTRATION

APPENDIX B

Simulation Program Listing

.Programming Language - PASCAL

```
(*$S+*)
PROGRAM A7;

USES TRANSCEND;

CONST   Tdelta = 0.05;
        Tint = 0.1;

TYPE   VECTOR = ARRAY[1..30] OF REAL;

VAR XO,Xfinal,F : VECTOR;
    Qbar,Qdot,adot,Antgt,Ptgt,Lazimuth,Lelevation,TO,Tfinal,Alpha,Beta,
    PILOTelev,PILOTail,PILOTrud,Cx,Cl,Cm,Cn,An,Ay,Rdot,Pdot : REAL;
    II,N,J,I,K,COUNT : INTEGER;
    b : CHAR;
    diskfile : STRING;
    OUTPUT : FILE OF RECORD
                STATE :VECTOR;
                Normalaccel,Tgtaccel,azimuth,elevation,Sideaccel,
                AOA,Sideslip,Time : REAL;
                END;


PROCEDURE COEFFICIENTS(VAR X: VECTOR;adot :REAL; VAR Qbar,Alpha,
                       Beta,Cx,Cl,Cm,Cn,An,Ay : REAL);
(* This procedure computes the force and moment coefficients for the A7 *)
(* DIGITAC aircraft.  The angular units are radians and the accelerat-  *)
(* ions are in ft/sec/sec.  The sign convention is positive for nose up *)
(* nose right, and roll right.  The positive control movements are      *)
(* elevator trailing edge down, right aileron up, and rudder trailing   *)
(* edge left.                                                           *)

CONST   k = 0.0194;        (* 1/ pi * AR * oswald's efficiency (80%) *)
        mass = 786.89;
        ClO = 0.174;
        Clalpha = 4.412;
        Cladot = 0.0;        (* actually Clalphadot *)
        Clq = 1.0;
        Clde = 0.596;
        CdO = 0.0219;
        Cybeta = -0.7162;
        Cyp = 0.129;
        Cyr = 0.3096;
        Cyda = -0.0502;
        Cydr = 0.2006;
        Clbeta = -0.0905;
        Clp = -0.346;
        Clr = 0.104;
        Clda = 0.1210;
        Cldr = 0.0190;
        Cmalpha = -0.4636;
        Cmadot = -0.77;        (* actually Cmalphadot  *)
```

75

```
            Cmq = -3.95;
            Cmde = -0.9056;
            Cnbeta = 0.0722;
            Cnp = -0.00397;
            Cnr = -0.302;
            Cnda = 0.0142;
            Cndr = -0.0917;
            chord = 10.84;        (*   feet   *)
            span = 38.73;         (*   feet   *)
            Wingarea = 375.0;     (*   square feet  *)
            rho = 0.001497;       (*   15,000 ft. MSL    slug/cubic ft. *)


    VAR Clift,Cdrag,Cy,Cz : REAL;




    (* F[i] is the time derivative of X[i]                              *)
    (* X[1] = U                          X[17] = demanual              *)
    (* X[2] = V                          X[18] = deelectric            *)
    (* X[3] = W                          X[19] = de                    *)
    (* X[4] = P                          X[20] = da1manual             *)
    (* X[5] = Q                          X[21] = da2manual             *)
    (* X[6] = R                          X[22] = da3electric           *)
    (* X[7] = Phi                        X[23] = da4electric           *)
    (* X[8] = Theta                      X[24] = da                    *)
    (* X[9] = Psi                        X[25] = rdot feedback         *)
    (* X[10]= Target Velocity            X[26] = Ay1                   *)
    (* X[11]= Target Psi                 X[27] = Ay2                   *)
    (* X[12]= Target Theta               X[28] = dr                    *)
    (* X[13]= Target Phi                                               *)
    (* X[14]= Relative Pos. - X                                        *)
    (* X[15]= Relative Pos. - Y                                        *)
    (* X[16]= Relative Pos. - Z                                        *)



    BEGIN
      Qbar:=(0.5)*rho*(X[1]*X[1]+X[2]*X[2]+X[3]*X[3]);
      Alpha:=X[3]/SQRT(X[1]*X[1]+X[2]*X[2]+X[3]*X[3]);
      Beta:=X[2]/SQRT(X[1]*X[1]+X[2]*X[2]);
      Clift:=Cl0 + Clalpha*Alpha + Cladot*((adot*chord)/(2*X[1])) + Clq*(
              (X[5]*chord)/(2*X[1])) + Clde*X[19];
      Cdrag:=Cd0 + k*Clift*Clift;
      Cx:= -Cdrag*cos(Alpha) + Clift*sin(Alpha);
      Cy:=Cybeta*Beta + Cyp*((X[4]*span)/(2*X[1])) + Cyr*((X[6]*span)/(2*X[1]))
          + Cyda*X[24] + Cydr*X[28];
      Cz:= -Cdrag*sin(Alpha) - Clift*cos(Alpha);
      Cl:=Clbeta*Beta + Clp*((X[4]*span)/(2*X[1])) + Clr*((X[6]*span)/(2*X[1]))
          + Clda*X[24] + Cldr*X[28];
      Cm:=Cmalpha*Alpha + Cmadot*((adot*chord)/(2*X[1])) + Cmq*((X[5]*chord)
```

76

```
                  /(2*X[1])) + Cmde*X[19];
    Cn:=Cnbeta*Beta + Cnp*((X[4]*span)/(2*X[1])) + Cnr*((X[6]*span)/(2*X[1]))
          + Cnda*X[24] + Cndr*X[28];
    An:= -(Qbar*Wingarea*Cz)/mass;
    Ay:= (Qbar*Wingarea*Cy)/mass;
    END;


  PROCEDURE A7DYN(VAR X: VECTOR;Qbar,Alpha,Cx,Cl,Cm,Cn,An,Ay : REAL;
                  VAR F: VECTOR;VAR adot : REAL);

  CONST   gravity = 32.2 ;
          I1 = -0.03413;
          I2 = 0.62048;
          I3 = 0.000065232;
          I4 = -0.000001374;
          I5 = -0.9153146;
          I6 = -0.023933;
          I7 = 0.0000143;
          I8 = -0.684845;
          I9 = -0.0341306;
          I10= -0.000001374;
          I11= 0.00001269;
          mass = 786.89;
          chord = 10.84;
          span = 38.73;
          Wingarea = 375.0;
          Thrust = 3272.0;
          WO = 40.0;             (* Initial AOA - trim W velocity *)


  BEGIN
    (*  A/C FORCE EQUATIONS    *)

    F[1]:=X[2]*X[6] - (X[3]+WO)*X[5] - gravity*sin(X[8]) +
          (Qbar*Wingarea*Cx)/(mass) + Thrust/mass;
    F[2]:=(X[3]+WO)*X[4] - X[1]*X[6] + gravity*sin(X[7])*cos(X[8]) + Ay;
    F[3]:=X[1]*X[5] - X[2]*X[4] + gravity*cos(X[7])*cos(X[8]) - An;
    adot:=F[3]/X[1] - Alpha*(F[1]/X[1]);

    (*  A/C MOMENT EQUATIONS   *)

    F[4]:=I1*X[4]*X[5] - I2*X[5]*X[6] + I3*Qbar*Wingarea*span*Cl + I4*
          Qbar*Wingarea*span*Cn;
    F[5]:=(-I5)*X[4]*X[6] - I6*(X[4]*X[4]-X[6]*X[6]) + Qbar*Wingarea*chord
          *Cm*I7;
    F[6]:=I8*X[4]*X[5] - I9*X[5]*X[6] + I10*Qbar*Wingarea*span*Cl + I11*
          Qbar*Wingarea*span*Cn;

    (*  A/C KINEMATIC EQUATIONS  *)

    F[7]:=X[4] + X[5]*sin(X[7])*sin(X[8])/cos(X[8]) + X[6]*cos(X[7])*
```

77

```
          /(2*X[1])) + Cmde*X[19];
    Cn:=Cnbeta*Beta + Cnp*((X[4]*span)/(2*X[1])) + Cnr*((X[6]*span)/(2*X[1]))
          + Cnda*X[24] + Cndr*X[28];
    An:= -(Qbar*Wingarea*Cz)/mass;
    Ay:= (Qbar*Wingarea*Cy)/mass;
    END;


  PROCEDURE A7DYN(VAR X: VECTOR;Qbar,Alpha,Cx,Cl,Cm,Cn,An,Ay : REAL;
                  VAR F: VECTOR;VAR adot : REAL);

  CONST   gravity = 32.2 ;
          I1 = -0.03413;
          I2 = 0.62048;
          I3 = 0.000065232;
          I4 = -0.000001374;
          I5 = -0.9153146;
          I6 = -0.023933;
          I7 = 0.0000143;
          I8 = -0.684845;
          I9 = -0.0341306;
          I10= -0.000001374;
          I11= 0.00001269;
          mass = 786.89;
          chord = 10.84;
          span = 38.73;
          Wingarea = 375.0;
          Thrust = 3272.0;
          WO = 40.0;              (* Initial AOA - trim W velocity *)


  BEGIN
    (*   A/C FORCE EQUATIONS   *)

    F[1]:=X[2]*X[6] - (X[3]+WO)*X[5] - gravity*sin(X[8]) +
          (Qbar*Wingarea*Cx)/(mass) + Thrust/mass;
    F[2]:=(X[3]+WO)*X[4] - X[1]*X[6] + gravity*sin(X[7])*cos(X[8]) + Ay;
    F[3]:=X[1]*X[5] - X[2]*X[4] + gravity*cos(X[7])*cos(X[8]) - An;
    adot:=F[3]/X[1] - Alpha*(F[1]/X[1]);

    (*   A/C MOMENT EQUATIONS   *)

    F[4]:=I1*X[4]*X[5] - I2*X[5]*X[6] + I3*Qbar*Wingarea*span*Cl + I4*
          Qbar*Wingarea*span*Cn;
    F[5]:=(-I5)*X[4]*X[6] - I6*(X[4]*X[4]-X[6]*X[6]) + Qbar*Wingarea*chord
          *Cm*I7;
    F[6]:=I8*X[4]*X[5] - I9*X[5]*X[6] + I10*Qbar*Wingarea*span*Cl + I11*
          Qbar*Wingarea*span*Cn;

    (*   A/C KINEMATIC EQUATIONS   *)

    F[7]:=X[4] + X[5]*sin(X[7])*sin(X[8])/cos(X[8]) + X[6]*cos(X[7])*
```

```
            sin(X[8])/cos(X[8]);
    F[8]:=X[5]*cos(X[7]) - X[6]*sin(X[7]);
    F[9]:=X[5]*sin(X[7])/cos(X[8]) + X[6]*cos(X[7])/cos(X[8]);
    END;


PROCEDURE ASSIGN(VAR F: VECTOR; VAR Pdot, Qdot, Rdot :REAL);

BEGIN
    Pdot:=F[4];
    Qdot:=F[5];
    Rdot:=F[6];
END;




PROCEDURE TGTDYN(VAR X: VECTOR; VAR F: VECTOR;
                    VAR Lazimuth,Lelevation,Antgt : REAL);


CONST  gravity = 32.2;

VAR Ph1,Ph2,T1,T2,Ps1,Ps2,PsT1,PsT2,TT1,TT2,PhT1,PhT2 : REAL;

BEGIN
    (*   TARGET DYNAMICS  *)

    Ph1:=cos(X[7]);
    Ph2:=sin(X[7]);
    T1:=cos(X[8]);
    T2:=sin(X[8]);
    Ps1:=cos(X[9]);
    Ps2:=sin(X[9]);
    PsT1:=cos(X[11]);
    PsT2:=sin(X[11]);
    TT1:=cos(X[12]);
    TT2:=sin(X[12]);
    PhT1:=cos(X[13]);
    PhT2:=sin(X[13]);

    Antgt:=gravity/PhT1;            (* Assuming a level turn *)
    F[10]:=0.0;
    F[11]:=(Antgt*PhT2)/(X[10]*TT1);
    F[12]:=(Antgt*PhT1-gravity*TT1)/X[10];
    F[13]:=Ptgt;

    (*   RELATIVE KINEMATICS  *)

    F[14]:=X[6]*X[15] - X[5]*X[16] + X[10]*((TT1*PsT1*T1*Ps1) + (TT1*PsT2
            *T1*Ps2) + (TT2*T2)) - X[1];
    F[15]:=-X[6]*X[14] + X[4]*X[16] + X[10]*(((PsT1*TT1)*(Ps1*Ph2*T2 - Ps2
            *Ph1)) + ((TT1*PsT2)*(Ps2*Ph2*T2 + Ps1*Ph1)) - (TT2*T1*Ph2)) - X[2]
    F[16]:=X[5]*X[14] - X[4]*X[15] + X[10]*(((PsT1*TT1)*(Ps1*Ph1*T2 + Ps2*
```

78

```pascal
          Ph2)) + ((TT1*PsT2)*(Ps2*Ph1*T2 - Ph2*Ps1)) - (TT2*T1*Ph1)) - X[3
    Lazimuth:=atan(X[15]/X[14]);
    Lelevation:=atan(-X[16]/X[14]);
    END;


  PROCEDURE ELEVATOR(VAR X: VECTOR;An,Qdot,PILOTelev : REAL;
                     VAR F: VECTOR);

  CONST  gvslb = 0.3;

  VAR kfs,de1,decommand :REAL;

  BEGIN

    (*  ELEVATOR - X[19] is the elevator movement (ie. delta e )   *)

    IF ABS(PILOTelev) < 8 THEN
      kfs:=ABS(PILOTelev)/32
      ELSE
      kfs:=0.25 + (ABS(PILOTelev) - 8)*0.344;
    de1:=PILOTelev - 0.00149*(An-32.2) - 0.167*Qdot;
    F[17]:=(-0.5*kfs)*X[17] + 0.5*de1;
    F[18]:=(-X[18] - (An-32.2) + 10*PILOTelev)*1.818;
    decommand:=X[17] + (X[18]-460*X[5])*0.00054;
    IF decommand > 0.262 THEN decommand:= 0.262
       ELSE
          IF decommand < -0.262 THEN decommand:=-0.262;
    F[19]:=-20*X[19] - 20*decommand;
  END;


  PROCEDURE AILERON(VAR X: VECTOR; PILOTail :REAL; VAR F: VECTOR);

  VAR dacommand : REAL;

  BEGIN

    (*  AILERON - X[24] is the aileron movement (ie. delta a )   *)

    F[20]:=-12.8*X[20] + 2*PILOTail;
    F[21]:=-12.5*X[21] + 1.24*X[20];
    F[22]:=-3.33*X[22] + 0.70*PILOTail;
    F[23]:=-10*X[23] + 10*X[22];
    dacommand:= (X[23]-X[4])*0.1;
    IF dacommand > 0.175 THEN dacommand:=0.175
      ELSE
         IF dacommand < -0.175 THEN dacommand:= -0.175;
    F[24]:=-20*X[24] + 20*dacommand + 20*X[21];
  END;
```

```
PROCEDURE RUDDER(VAR X: VECTOR; PILOTrud, Ay, Rdot : REAL;
                 VAR F: VECTOR);

VAR k1, dr1, dr2, drcommand, drpilot :REAL;

BEGIN

  (*  RUDDER - X[28] is the rudder movement (ie. delta r )  *)

  dr1:=0.0;    (* Initialize dr1 *)
  (* 14 lb breakout force *)
  IF ABS(PILOTrud) < 14 THEN PILOTrud:=0.0
     ELSE IF PILOTrud > 14 THEN PILOTrud:=PILOTrud-14.0
             ELSE IF PILOTrud < -14 THEN PILOTrud:=PILOTrud + 14.0;
  drpilot:=0.001064*PILOTrud;
  (* 6 degree pilot rudder command limit in cruise *)
  IF drpilot > 0.105 THEN drpilot:=0.105
     ELSE IF drpilot < -0.105 THEN drpilot:=-0.105;
  (* ARI is scheduled with elevator (X[19]).                      *)
  (* Normally, the ARI is ramp scheduled with elevator between *)
  (* -4.5 and 1.5 degrees elevator movement and a constant        *)
  (* + or - 0.2 outside of those values.  Because the trim        *)
  (* elevator position for this flight condition (350 KIAS,       *)
  (* 15,000 feet PA) is approximately -4.5 degrees, the ramp      *)
  (* start and stop points have been shifted to reflect a trim *)
  (* elevator position at -4.5 degrees.                           *)
  IF X[19] < 0.0 THEN
     k1:=1.0
     ELSE
     IF X[19] > 0.10471 THEN
        k1:=-1.0
        ELSE
        k1:=-0.5 - (X[19]-0.07853)*19.1;
  F[25]:=-X[25] + 0.25*Rdot;
  dr2:=(-0.2*k1*X[24]);
  IF ABS(drpilot)<0.02 THEN
     Begin
        F[26]:=-2*X[26] + 2*Ay;
        F[27]:=0.0009*X[26];
        dr1:=0.003*X[26] + X[27];
           IF dr1 > 0.07 THEN dr1:=0.07
               ELSE IF dr1 < -0.07 THEN dr1:=-0.07;
     End;
  drcommand:=X[25] + dr1 + dr2 + drpilot;
  IF drcommand>0.24 THEN drcommand:=0.24
     ELSE
     IF drcommand<-0.24 THEN drcommand:=-0.24;
  F[28]:=-33.3*X[28] + 33.3*drcommand;
END;


PROCEDURE XPRIME(VAR X: VECTOR; VAR F: VECTOR);
```

```
      BEGIN
        COEFFICIENTS(X,adot,Qbar,Alpha,Beta,Cx,Cl,Cm,Cn,An,Ay);
        A7DYN(X,Qbar,Alpha,Cx,Cl,Cm,Cn,An,Ay,F,adot);
        ASSIGN(F,Pdot,Qdot,Rdot);
        TGTDYN(X,F,Lazimuth,Lelevation,Antgt);
        ELEVATOR(X,An,Qdot,PILOTelev,F);
        AILERON(X,PILOTail,F);
        RUDDER(X,PILOTrud,Ay,Rdot,F);
      END;


      PROCEDURE PRINTOUT(VAR T:REAL; X : VECTOR);

      VAR I :  INTEGER;
          J :  REAL;
          b :  CHAR;
          F :  INTERACTIVE;

      BEGIN
        WRITELN(T);
        J:=COUNT*Tint - 0.01;
        IF T<J   THEN EXIT(PRINTOUT)
         ELSE
         IF COUNT=1 THEN
         BEGIN
           WITH OUTPUT^ DO
           FOR I:=1 TO 30 DO STATE[I]:=0.0;
         END;
         COUNT:=COUNT+1;
         WITH OUTPUT^ DO
         Begin
           FOR I:=1 TO 30 DO STATE[I]:=X[I];
           Normalaccel:=An;
           Tgtaccel:=Antgt;
           azimuth:=Lazimuth;
           elevation:=Lelevation;
           Sideaccel:=Ay;
           AOA:=Alpha;
           Sideslip:=Beta;
           Time:=T;
         End;
         PUT(OUTPUT);
      END;


      PROCEDURE RKDF(VAR X0:VECTOR; T0,Tfinal,Tdelta:REAL; N:INTEGER;
                     VAR Xfinal: VECTOR);

      (* This procedure is a fourth-order Runge-kutta Diffe......
      (* solver. (Ref: Numerical Methods, Robert Hornbeck.......
      (* It requires a TYPE declaration in the main prog..  .
```
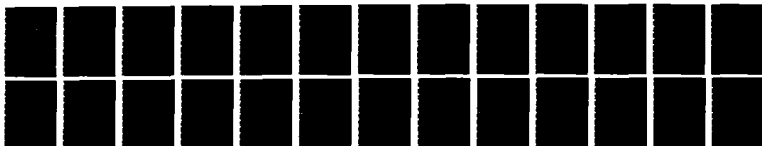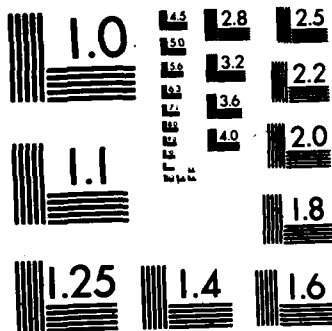
81

MICROCOPY RESOLUTION TEST CHART

NATIONAL BUREAU OF STANDARDS-1963-A

```
(* VECTOR = ARRAY[1..10] OF REAL                                          *)
(* and a VAR declaration for the parameters in the above parameter        *)
(* list.  It also requires a procedure XPRIME and PRINTOUT.  The          *)
(* XPRIME procedure contains the equations to be solved.  The             *)
(* PRINTOUT procedure contains the output format.                         *)


VAR I,K,NN : INTEGER;
    X1,X2,X3,F0,F1,F2,F3: VECTOR;
    Iterations, Tend, Tbidelta, Thexdelta : REAL;

BEGIN    (* RKDF  *)
  FOR I := 1 TO 30 DO
    F0[I]:=0.0;
  Tend := T0;
  Tbidelta := Tdelta/2;
  Thexdelta := Tdelta/6;
  Iterations := (Tfinal - T0)/Tdelta;
  NN := ROUND(Iterations);
  FOR K := 1 TO NN DO
    BEGIN   (* K - Loop *)
      XPRIME(X0,F0);
      FOR I := 1 TO N DO
        X1[I] := X0[I] + (Tbidelta)*F0[I];
      XPRIME(X1,F1);
      FOR I := 1 TO N DO
        X2[I] := X0[I] + (Tbidelta)*F1[I];
      XPRIME(X2,F2);
      FOR I := 1 TO N DO
        X3[I] := X0[I] + Tdelta*F2[I];
      XPRIME(X3,F3);
      Tend := Tend + Tdelta;
      FOR I := 1 TO N DO
        Begin
          Xfinal[I] := X0[I] + (Thexdelta)*(F0[I] + 2*(F1[I] + F2[I]) +
                                      F3[I]);

          X0[I] := Xfinal[I];
        End;
      PRINTOUT(Tend,Xfinal);
    END;  (* K - Loop *)
  END;   (* RKDF *)



BEGIN     (*  MAIN PROGRAM  *)
(* INITIALIZE VARIABLES  *)
  FOR II:= 1 TO 30 DO
    Begin
      F[II]:=0.0;
      X0[II]:=0.0;
    End;
```

82

```
      Qbar:=0.0;
      Pdot:=0.0;
      Qdot:=0.0;
      Rdot:=0.0;
      adot:=0.0;
      Antgt:=32.2;
      Ptgt:=0.0;
      PILOTelev:=0.0;
      PILOTail:=0.0;
      PILOTrud:=0.0;
      Lazimuth:=0.0;
      Lelevation:=0.0;
      Cx:=0.0;
      Cl:=0.0;
      Cm:=0.0;
      Cn:=0.0;
      An:=0.0;
      Ay:=0.0;
      N:=28;
      b:=' ';
      COUNT:=1;
      (* END INITIALIZATION *)
      Writeln(' If you want any NONzero state values, enter them one ');
      Writeln(' at a time when prompted by first entering the number ');
      Writeln(' of the state, a space, then the value. ');
      Writeln(' (eg. XO[10]=-4 would be  10 -4<return> ');
      REPEAT
        Write(' Input the state number and value (zero when done) ');
        Read(J);
        IF (J<0) OR (J>N) THEN Writeln(' Reenter ')
          ELSE
            IF J=0 THEN Writeln
              ELSE
                Readln(XO[J]);
      UNTIL J=0;
      Write(' Enter PILOTail = ');
      Readln(PILOTail);
      Write(' Enter PILOTrud = ');
      Readln(PILOTrud);
      Write(' Enter initial time = ');
      Readln(TO);
      Write(' Enter final time = ');
      Readln(Tfinal);
      Write(' Name of output file: ');
      Readln(diskfile);
      IF LENGTH(diskfile)=0 THEN EXIT(PROGRAM);
      IF POS('.',diskfile)=0 THEN diskfile:=CONCAT(diskfile,'.DATA');
      REWRITE(OUTPUT,diskfile);
      RKDF(XO,TO,Tfinal,Tdelta,N,Xfinal);
      CLOSE(OUTPUT,LOCK);
    END.    (*  MAIN PROGRAM  *)
```

```
PROGRAM PRINT;

TYPE VECTOR = ARRAY[1..30] OF REAL;

VAR I,COUNT : INTEGER;
    J,An,Ay,Beta,T : REAL;
    b : CHAR;
    diskfile : STRING;
    X : VECTOR;
    F : INTERACTIVE;
    INPUT : FILE OF RECORD
              STATE : VECTOR;
              Normalaccel,Tgtaccel,azimuth,elevation,Sideaccel,
              AOA,Sideslip,Time : REAL;
              END;

BEGIN
    Write('Name of input file: ');
    Readln(diskfile);
    IF LENGTH(diskfile)=0 THEN EXIT(PROGRAM);
    IF POS('.',diskfile)=0 THEN
      diskfile:=CONCAT(diskfile,'.DATA');
    COUNT:=1;
    RESET(INPUT,diskfile);
    IF COUNT=1 THEN
    BEGIN
    b:=' ';
    REWRITE(F,'PRINTER:');
    Writeln(F,CHR(15));
    Write(F,' T ',b:7,'U',b:7,'V',b:7,'W',b:7,'P',b:7,'Q');
    Write(F,b:8,'R',b:6,'PHI',b:3,'THETA',b:3,'PSI',b:6,'de',b:6,'da',b:6);
    Writeln(F,'dr',b:6,'An',b:7,'Ay',b:3,'Beta',CHR(18));
    CLOSE(F);
    END;
    REWRITE(F,'PRINTER:');
    Writeln(F,CHR(15));
    REPEAT
    IF COUNT>1 THEN GET(INPUT);
    WITH INPUT^ DO
     Begin
       FOR I:= 1 TO 9 DO X[I]:=STATE[I];
       X[19]:=STATE[19];
       X[24]:=STATE[24];
       X[28]:=STATE[28];
       T:=Time;
       An:=Normalaccel;
       Ay:=Sideaccel;
       Beta:=Sideslip;
     End;
    COUNT:=COUNT+1;
    Write(F,T:3:1,X[1]:8:4,X[2]:8:5,X[3]:8:5,X[4]:8:5,X[5]:8:5,X[6]:8:5);
    Write(F,X[7]:8:5,X[8]:8:5,X[9]:8:5,X[19]:8:5,X[24]:8:5,X[28]:8:5);
```

84

```
      Writeln(F,An:8:5,Ay:8:5,Beta:8:5);
   UNTIL EOF(INPUT);
   Writeln(F,CHR(18));
   CLOSE(F);
END.
```

APPENDIX C

Development of Target Dynamics and Relative Kinematics

# DEVELOPMENT OF TARGET DYNAMICS AND RELATIVE KINEMATIC EQUATIONS

The target was modelled as a point mass with a velocity and angular orientations. The angular orientations were necessary since they provide important feedback cues to the pilot for the air-to-air tracking task. For example, the pilot needs to know the bank angle of the target so that he can match his bank angle to the target to be able to stay in the target turning plane, or at least in a parallel turning plane. Actually, for the tracking task, the pilot only needs to know the relative difference in angular orientations between his aircraft and the target. The absolute orientation is of use for air-to-air tracking "situation awareness" (ie. present and future energy states).

The following equation developments for the target dynamics and relative kinematics are provided as support for the discussions in the body of this report.

TARGET DYNAMICS

The first step in describing the relative motion between two bodies in motion, is to reference their motion to a fixed (inertial) reference frame. For the air-to-air tracking task, the earth surface fixed reference frame will suffice as an equivalent inertial frame. The target can be referenced to the earth fixed frame through a sequence of three rotations.

Assume $\hat{e}_1, \hat{e}_2, \hat{e}_3$ = orthogonal earth fixed unit vectors

$\hat{v}_1, \hat{v}_2, \hat{v}_3$ = orthogonal target fixed unit vectors
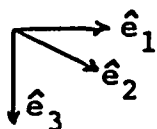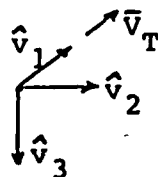
$$\bar{V}_T = V\hat{v}_1$$
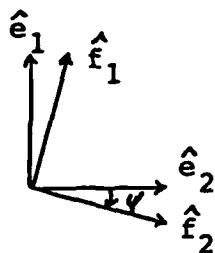
$\hat{v}_3$ is normal to the target wings.

The three rotations will be:

ψ about $\hat{e}_3$ to define $\hat{f}_1, \hat{f}_2, \hat{f}_3$

θ about $\hat{f}_2$ to define $\hat{g}_1, \hat{g}_2, \hat{g}_3$

ϕ about $\hat{g}_1$ to define $\hat{v}_1, \tilde{v}_2, \hat{v}_3$
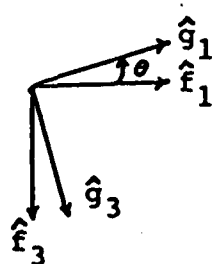
Top View

$$[C^{fe}] = \begin{bmatrix} \cos\psi & \sin\psi & 0 \\ -\sin\psi & \cos\psi & 0 \\ 0 & 0 & 1 \end{bmatrix}$$

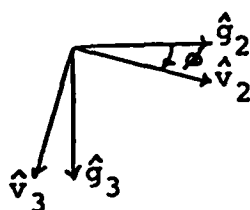$$\bar{w}^{fe} = \dot{\psi}\,\hat{e}_3 = \dot{\psi}\,\hat{f}_3$$

Side View

$$[C^{gf}] = \begin{bmatrix} \cos\theta & 0 & -\sin\theta \\ 0 & 1 & 0 \\ \sin\theta & 0 & \cos\theta \end{bmatrix}$$

$$\bar{w}^{gf} = \dot{\theta}\hat{f}_2 = \dot{\theta}\hat{g}_2$$

Tail View

$$[C^{vg}] = \begin{bmatrix} 1 & 0 & 0 \\ 0 & \cos\phi & \sin\phi \\ 0 & -\sin\phi & \cos\phi \end{bmatrix}$$

$$\bar{w}^{vg} = \dot{\phi}\hat{g}_1 = \dot{\phi}\hat{v}_1$$

To find $\bar{A}_T{}^e$:

$$\bar{A}_T{}^e = \frac{^e d}{dt}(\bar{V}_T) = \frac{^e d}{dt}(v\hat{v}_1) = \frac{^v d}{dt}(v\hat{v}_1) + \bar{w}^{ve} \times (v\hat{v}_1)$$

$$= \dot{v}\hat{v}_1 + (\dot{\phi}\hat{v}_1 + \dot{\theta}\hat{g}_2 + \dot{\psi}\hat{f}_3) \times (v\hat{v}_1)$$

Using the relationships defined above to transform the $\hat{g}_2$ and $\hat{f}_3$ terms into $\hat{v}$ coordinates, we get:

$$\bar{A}_T{}^e = \dot{v}\hat{v}_1 + (\dot{\phi}\hat{v}_1 + \dot{\theta}\cos\phi\hat{v}_2 - \dot{\theta}\sin\phi\hat{v}_3 - \dot{\psi}\sin\theta\hat{v}_1 + \dot{\psi}\cos\theta\sin\phi\hat{v}_2$$
$$+ \dot{\psi}\cos\theta\cos\phi\hat{v}_3) \times v\hat{v}_1$$
$$= \dot{v}\hat{v}_1 + (v\dot{\psi}\cos\theta\cos\phi - v\dot{\theta}\sin\phi)\hat{v}_2 + (-v\dot{\theta}\cos\phi$$
$$- v\dot{\psi}\cos\theta\sin\phi)\hat{v}_3$$

$$[C^{ev}] = [C^{ef}][C^{fg}][C^{gv}]$$

$$= \begin{bmatrix} \cos\psi\cos\theta & -\sin\psi\cos\theta + \sin\theta\cos\psi\sin\phi & \sin\phi\sin\psi + \\ & & \sin\theta\cos\psi\cos\phi \\ & & \\ \cos\theta\sin\psi & \cos\phi\cos\psi + \sin\theta\sin\psi\sin\phi & -\cos\psi\sin\phi + \\ & & \sin\theta\sin\psi\cos\phi \\ & & \\ -\sin\theta & \cos\theta\sin\phi & \cos\theta\cos\phi \end{bmatrix}$$

Now using $\bar{F} = m\bar{A}$ to get the target equations of motion.
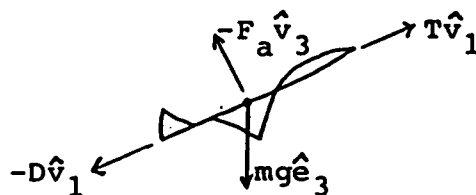
$$mg\hat{e}_3 = mg(-\sin\theta\hat{v}_1 + \cos\theta\sin\phi\hat{v}_2 + \cos\theta\cos\phi\hat{v}_3)$$

$\hat{v}_1$: $\quad m\dot{V} = T - D - mg\sin\theta$

$\hat{v}_2$: $\quad (V\dot{\psi}\cos\theta\cos\phi - V\dot{\theta}\sin\phi) = g\cos\theta\sin\phi$

$\hat{v}_3$: $\quad -(V\dot{\theta}\cos\phi - V\dot{\psi}\cos\theta\sin\phi) = g\cos\theta\cos\phi - F_a/m$

assume $\quad \dot{V} = 0, \quad \dot{\phi} = P_{tgt} = $ given, $\quad F_a/m = $ given (target "g")

To solve for $\dot{\psi}$, solve the $\hat{v}_2$ equation for $V\dot{\theta}$ and substitute into the $\hat{v}_3$ equation. Then through algebraic manipulations:

90

$$\dot{\psi} = \frac{F_a/m \sin\phi}{V \cos\theta}$$

Substituting this back into the $V\dot{\theta}$ equation and solving for $\dot{\theta}$:

$$\dot{\theta} = \frac{Fa/m \cos\phi - g\cos\theta}{V}$$

Relative Kinematics

Refering to figure 4, the vector of interest for the relative kinematics is $\bar{r}_{T/A}$ (the position of the target with respect to the attacker). In the earth fixed frame:

$$\bar{r}_{T/A} = x\hat{e}_1 + y\hat{e}_2 + z\hat{e}_3$$

$$\frac{^ed}{dt}(\bar{r}_{T/A}) = \bar{V}_T^e - \bar{V}_A^e = V_T\hat{v}_1 - (U\hat{b}_1 + V\hat{b}_2 + W\hat{b}_3)$$

$$\begin{bmatrix} \dot{x} \\ \dot{y} \\ \dot{z} \end{bmatrix}_e = [C^{ev}] \begin{bmatrix} V_T \\ 0 \\ 0 \end{bmatrix}_v - [C^{eb}] \begin{bmatrix} U \\ V \\ W \end{bmatrix}_b$$

The desired quantity is the motion of the target with respect to the attacker. Therefore, describing $r_{T/A}$ in the attacker body frame:

$$\bar{r}_{T/A} = r_1\hat{b}_1 + r_2\hat{b}_2 + r_3\hat{b}_3$$

$$\frac{^e d}{dt}(\bar{r}_{T/A}) = \frac{^b d}{dt}(\bar{r}_{T/A}) + \bar{w}^{be} \times \bar{r}_{T/A}$$

Solving for $\frac{^b d}{dt}(\bar{r}_{T/A})$:

$$\frac{^b d}{dt}(\bar{r}^b_{T/A}) = \frac{^e d}{dt}(\bar{r}^e_{T/A}) - \bar{w}^{be} \times \bar{r}^b_{T/A}$$

$$\frac{^e d}{dt}(\bar{r}^e_{T/A}) = \bar{V}_T^e - \bar{V}_A^e$$

$$\bar{w}^{be} \times \bar{r}^b_{T/A} = \begin{bmatrix} 0 & -R & Q \\ R & 0 & -P \\ -Q & P & 0 \end{bmatrix}\begin{bmatrix} r_1 \\ r_2 \\ r_3 \end{bmatrix}$$

Therefore:

$$\begin{bmatrix} \dot{r}_1 \\ \dot{r}_2 \\ \dot{r}_3 \end{bmatrix}_b = -\begin{bmatrix} 0 & -R & Q \\ R & 0 & -P \\ -Q & P & 0 \end{bmatrix}\begin{bmatrix} r_1 \\ r_2 \\ r_3 \end{bmatrix}_b + [C^{be}][C^{ev}]\begin{bmatrix} V_T \\ 0 \\ 0 \end{bmatrix}_v - \begin{bmatrix} U \\ V \\ W \end{bmatrix}_b$$

The direction cosine matrix $[C^{ev}]$ was developed earlier. The matrix $[C^{be}]$ can be developed in the same manner. Using the same standard sequence of rotations, yaw, pitch, and roll, we obtain three direction cosine matrices which are combined to arrive at the overall direction cosine matrix ($[C^{be}]$).

92

$$[c^{be}] = [c^{bg}][c^{gf}][c^{fe}]$$

$$= \begin{bmatrix} \cos\theta\cos\psi & \sin\psi\cos\theta & -\sin\theta \\ \cos\psi\sin\phi\sin\theta - \sin\psi\cos\phi & \sin\psi\sin\phi\sin\theta + \cos\psi\cos\phi & \cos\theta\sin\phi \\ \cos\psi\cos\phi\sin\theta + \sin\psi\sin\phi & \sin\psi\cos\phi\sin\theta - \sin\phi\cos\psi & \cos\theta\cos\phi \end{bmatrix}$$

$$[c^{bv}] = [c^{be}][c^{ev}]$$

$$= \begin{bmatrix} c_{11} & c_{12} & c_{13} \\ c_{21} & c_{22} & c_{23} \\ c_{31} & c_{32} & c_{33} \end{bmatrix}$$

It's evident from the vector multiplier to $[c^{bv}]$, that only the first column of $[c^{bv}]$ is of interest. The subscript T is used here to distinguish target angles from attacker angles.

$$c_{11} = \cos\psi_T\cos\theta_T\cos\theta\cos\psi + \cos\theta_T\sin\psi_T\sin\psi\cos\theta + \sin\theta_T\sin\theta$$

$$c_{21} = \cos\psi_T\cos\theta_T\cos\psi\sin\phi\sin\theta - \cos\psi_T\cos\theta_T\sin\psi\cos\phi$$
$$+ \cos\theta_T\sin\psi_T\sin\psi\sin\phi\sin\theta + \cos\theta_T\sin\psi_T\cos\psi\cos\phi$$
$$- \sin\theta_T\cos\theta\sin\phi$$

$$c_{31} = \cos\psi_T\cos\theta_T\cos\psi\sin\theta + \cos\psi_T\cos\theta_T\sin\psi\sin\phi$$
$$+ \cos\theta_T\sin\psi_T\sin\psi\cos\phi\sin\theta - \sin\psi_T\cos\theta_T\cos\psi\sin\phi$$
$$- \sin\theta_T\cos\theta\cos\phi$$

Therefore:

$$\dot{r}_1 = Rr_2 - Qr_3 + c_{11}V_T - U$$
$$\dot{r}_2 = -Rr_1 + Pr_3 + c_{21}V_T - V$$
$$\dot{r}_3 = Qr_1 - Pr_2 + c_{31}V_T - W$$

To describe how the target would appear in the attacker HUD:

λ_a = azimuth angle of target in HUD

$\quad$ = arctan (r_2/r_1)

λ_e = elevation angle of target in HUD

$\quad$ = arctan $(-r_3/r_1)$

APPENDIX D

Development of Linear Equations

DEVELOPMENT OF LINEAR EQUATIONS

In this section the details of developing the linear model of the air-to-air lateral-directional tracking task are shown along with the linear mechanical and CAS roll control system.

The starting point for the linear model of the lateral-directional air-to-air tracking task is the linearized lateral-directional equations of motion for the aircraft. The linearized equations were obtained from Roskam and are shown below.

$$\dot{\beta} = (1/U)(Y_\beta\beta + g\phi + Y_p p) + (Y_r/U - 1)r$$
$$+ (1/U)(Y_{\delta_a}\delta a + Y_{\delta_r}\delta_r)$$
$$\dot{p} = L'_\beta\beta + L'_p p + L'_r r + L'_{\delta_a}\delta a + L'_{\delta_r}\delta r$$
$$\dot{r} = N'_\beta\beta + N'_p p + N'_r r + N'_{\delta_a}\delta a + N'_{\delta_r}\delta r$$
$$\dot{\phi} = p$$

where

$$L'_a = [(L_a + (I_{xz}/I_{xx})N_a) / (1 - ((I_{xz})^2/I_{xx}I_{zz}))]$$
$$N'_a = [(N_a + (I_{xz}/I_{zz})L_a) / (1 - ((I_{xz})^2/I_{xx}I_{zz}))]$$

Arranging these equations in state variable form ($\dot{\bar{x}} = [A]\bar{x} + [B]\bar{u}$) where $\bar{x}^T = [\beta\ p\ r\ \phi]$ and $\bar{u}^T = [\delta_a\ \delta_r]$ we obtain the A matrix:

$$[A] = \begin{bmatrix} Y_\beta/U & Y_p/U & (Y_r/U - 1) & g/U \\ L'_\beta & L'_p & L'_r & 0 \\ N'_\beta & N'_p & N'_r & 0 \\ 0 & 1 & 0 & 0 \end{bmatrix}$$

and

$$[B] = \begin{bmatrix} Y_{\delta_a}/U & Y_{\delta_r}/U \\ L'_{\delta_a} & L'_{\delta_r} \\ N'_{\delta_a} & N'_{\delta_r} \\ 0 & 0 \end{bmatrix}$$

The stability parameters were obtained from an LTV report (Reference 6) and are shown in Table D1. Substituting in these values we get:

$$[A] = \begin{bmatrix} -0.162 & 0.00089 & -0.9979 & 0.05079 \\ -26.23 & -3.008 & 0.9596 & 0 \\ 4.546 & 0.05664 & -0.5298 & 0 \\ 0 & 1 & 0 & 0 \end{bmatrix}$$

$$[B] = \begin{bmatrix} -0.01132 & 0.0453 \\ 34.55 & 5.972 \\ 0.0614 & -5.307 \\ 0 & 0 \end{bmatrix}$$

Changing the state variable β to v where $v = \beta U$, we get a new state vector, $\bar{x}^T = [v\ p\ r\ \phi]$ and new plant and control matrices which differ from the previous matrices in that the first row of both matrices is multiplied by U and the first column of the plant matrix is divided by U. This was done primarily as a

97

TABLE D1
Lateral-Directional Stability Parameters

Y_β (ft/sec^2)	-102.6961
Y_p (ft/sec)	0.5643
Y_r (ft/sec)	1.3516
$Y_{\delta a}$ (ft-rad/sec^2)	-7.1836
$Y_{\delta r}$ (ft-rad/sec^2)	28.7641
L_β (sec^{-2})	-25.7350
L_p (sec^{-1})	-3.00146
L_r (sec^{-1})	0.9022
$L_{\delta a}$ (rad/sec)	34.3848
$L_{\delta r}$ (rad/sec)	5.4094
N_β (sec^{-2})	3.9938
N_p (sec^{-1})	-0.0067
N_r (sec^{-1})	-0.5096
$N_{\delta a}$ (rad/sec)	0.7854
$N_{\delta r}$ (rad/sec)	-5.0721

cosmetic change because the relative kinematic equation developed earlier contained a v term.

Next assume no rudder inputs to eliminate δ_r and add a roll attitude pilot model. The effect of this roll attitude pilot model is to couple the roll and spiral poles together and make them a complex conjugate pair with good damping and a fast response time. The roll attitude pilot model is realized by first closing an inner roll rate feedback loop and then using roll attitude feedback as the outer loop. This is illustrated in figure D1. Another effect of using roll attitude feedback is changing the control variable from δ_a to ϕ_c.

In figure D1, the transfer function p/δ_a is obtained from the A and B matrices shown earlier.

$$\frac{p}{\delta_a} = \frac{34.55 \ s \ (s + 0.351 + j2.13)}{(s + 0.036)(s + 0.34 \pm j2.1)(s + 3)}$$

To simplify, assume that the spiral effect is eliminated by the zero at the origin and that the dutch roll is not present due to the zeroes close by. This implies that the spiral and dutch roll are not prevalent in an aileron roll and that the response is primarily due to the roll mode root. This is true for most aircraft and is also true in the case of the A-7D. Thus, with the above simplifications:

$$\frac{p}{\delta_a} = \frac{35}{s + 3}$$

The values for K_p and K_ϕ were chosen to give good response and adequate damping. By choosing $K_p = 0.1$ and $K_\phi = 0.5$, we get the closed loop transfer function:
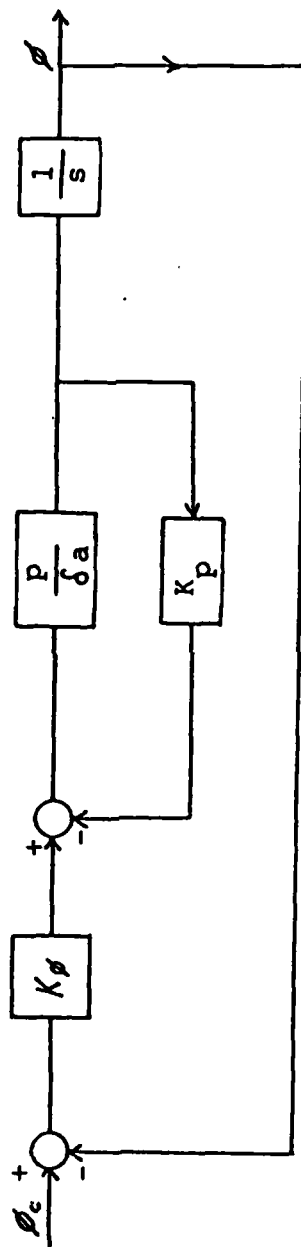
FIGURE D1: ROLL ATTITUDE PILOT MODEL

100

$$\frac{\phi}{\phi_c} = \frac{17.5}{s^2 + 6.5s + 17.5}$$

This yields a final value of one, a natural frequency of approximately four radians/second, and a damping of approximately 0.77 which are within the average pilot's abilities.

The inclusion of this roll attitude pilot model into the linear model was done by first writing the old control variable (δ_a) in terms of the new control variable (ϕ_c).

$$\delta_a = 0.5\phi_c - 0.5\phi - 0.1p$$

Next the feedback matrix (K) is used to obtain a new plant matrix.

$$[K] = [0 \quad 0.1 \quad 0 \quad 0.5]$$

$$[\tilde{A}] = [A] - [B][K]$$

$$[\tilde{A}] = \begin{bmatrix} -0.162 & 1.282 & -632.7 & 35.79 \\ -0.0414 & -6.463 & 0.9596 & -17.28 \\ 0.0072 & 0.0505 & -0.5298 & -0.0307 \\ 0 & 1 & 0 & 0 \end{bmatrix}$$

Note that here $\bar{x}^T = [v \ p \ r \ \phi]$.

u' = ϕ_c, therefore,

$$[B'] = 0.5[B]$$

$$[B'] = \begin{bmatrix} -3.588 \\ 17.28 \\ 0.0307 \\ 0 \end{bmatrix}$$

101

The next step was the addition of a yaw SAS to increase the dutch roll damping (ie. move the dutch roll poles away from the imaginary axis). To accomplish this, the yaw damping term (N_r', the 3,3 element of [A]) was artificially increased to -2.0. The effect was to increase the dutch roll damping from 0.16 to 0.50.

The modified linear aircraft model was then augmented with a heading term (ψ). The heading term was included since lateral-directional tracking involves lateral pointing which can be represented with heading angle.

$$\dot{\psi} = r$$

To this fifth order linear system was added a lateral relative kinematic term which represents the lateral tracking error. The equation used was a linearized version of the lateral element of the relative kinematic equations.

$$\dot{r}_2 = -rr_1 + pr_3 + V_T(-\psi) - v$$

We now have a sixth order state variable representation of the lateral-directional air-to-air tracking task.

$$\bar{x}^T = [\; v \; p \; r \; \phi \; \psi \; r_2 \;]$$

$$u = \phi_c$$

$$[A] = \begin{bmatrix} -0.162 & 1.282 & -632.7 & 35.79 & 0 & 0 \\ -0.0414 & -6.463 & 0.9596 & -17.28 & 0 & 0 \\ 0.0072 & 0.0505 & -2 & -0.0307 & 0 & 0 \\ 0 & 1 & 0 & 0 & 0 & 0 \\ 0 & 0 & 1 & 0 & 0 & 0 \\ -1 & -37.5 & -1500 & 0 & -634 & 0 \end{bmatrix}$$

102

Note: [A] is for 147 mil roll axis depression.

$$[B] = \begin{bmatrix} -3.585 \\ 17.28 \\ 0.0307 \\ 0 \\ 0 \\ 0 \end{bmatrix}$$

The linear model of the air-to-air tracking task does not contain any of the control system elements which, from the nonlinear analysis, have an effect on aircraft response to pilot inputs. The control systems could not be incorporated into the above linear model because of limitations on the size of state variable models in TOTAL. In order to compare the linear fourth order lateral-directional aircraft model to flight test, the linearized mechanical and CAS roll axis controls were added to the aircraft model. Referencing figure 2, the equations for the mechanical and CAS roll axis control are:

$$\dot{A}_1 = -3.33A_1 + 0.7F_{sa}$$

$$\dot{A}_2 = 10A_1 - 10A_2$$

$$\dot{A}_3 = -12.8A_3 + 2F_{sa}$$

$$\dot{A}_4 = 1.238A_3 - 12.5A_4$$

$$\delta_{ac} = 0.1A_2 - 0.1p + A_4$$

$$\dot{\delta}_a = 2A_2 - 2p + 20A_4 - 20\delta_a$$

The primary nonlinear element that was neglected in this representation was the series servo limit on the CAS authority. The new state vector is $\bar{x}^T = [\ v\ p\ r\ \phi\ A_1\ A_2\ A_3\ A_4\ \delta_a\ ]$, and the new control variable is lateral stick force (F_{sa}). The A matrix is shown on the next page. The B matrix is:

$$[B]^T = [\ 0\ \ 0\ \ 0\ \ 0\ \ 0.7\ \ 0\ \ 2\ \ 0\ \ 0\ ]$$

This is the ninth order linearized roll CAS model that was compared to flight test for p/F_{sa} frequency response.

$$[A] = \begin{bmatrix}
-0.1620 & 0.5643 & -632.7 & 32.2 & 0 & 0 & 0 & 0 & -7.176 \\
-0.0414 & -3.008 & 0.9596 & 0 & 0 & 0 & 0 & 0 & 34.55 \\
0.0072 & 0.05664 & -0.5298 & 0 & 0 & 0 & 0 & 0 & 0.0614 \\
0 & 1 & 0 & 0 & 0 & 0 & 0 & 0 & 0 \\
0 & 0 & 0 & 0 & -3.33 & 0 & 0 & 0 & 0 \\
0 & 0 & 0 & 0 & 10 & -10 & 0 & 0 & 0 \\
0 & 0 & 0 & 0 & 0 & 0 & -12.8 & 0 & 0 \\
0 & 0 & 0 & 0 & 0 & 0 & 1.238 & -12.5 & 0 \\
0 & -2 & 0 & 0 & 0 & 2 & 0 & 20 & -20
\end{bmatrix}$$

William L. Eischens was born in 1956 at Park Rapids, Minnesota. At the age of two months he moved to Adak, Alaska. He graduated from high school there in 1973 and went on to college at Parks College of St. Louis University in Cahokia, Illinois. In 1976, he graduated with a Bachelor of Science degree in Aeronautics and was commissioned in the U.S. Air Force.

His first assignment was as a Reliability and Maintainability Engineer at the Air Force Flight Test Center, Edwards AFB, California. There he worked on the B-1, F-16, ALCM, and KC-10 programs. He entered AFIT in the summer of 1981.

REPORT DOCUMENTATION PAGE		READ INSTRUCTIONS BEFORE COMPLETING FORM
1. REPORT NUMBER AFIT/GAE/AA/83S-2	2. GOVT ACCESSION NO.	3. RECIPIENT'S CATALOG NUMBER
4. TITLE (and Subtitle) Development and Flight Test Evaluation of an Analytical Model of the Air-to-Air Tracking Task		5. TYPE OF REPORT & PERIOD COVERED MS Thesis
		6. PERFORMING ORG. REPORT NUMBER
7. AUTHOR(s) William L. Eischens Captain, USAF		8. CONTRACT OR GRANT NUMBER(s)
9. PERFORMING ORGANIZATION NAME AND ADDRESS Air Force Institute of Technology (AFIT-EN) Wright-Patterson AFB OH 45433		10. PROGRAM ELEMENT, PROJECT, TASK AREA & WORK UNIT NUMBERS
11. CONTROLLING OFFICE NAME AND ADDRESS		12. REPORT DATE September 1983
		13. NUMBER OF PAGES 121
14. MONITORING AGENCY NAME & ADDRESS(if different from Controlling Office)		15. SECURITY CLASS. (of this report) Unclassified
		15a. DECLASSIFICATION/DOWNGRADING SCHEDULE

16. DISTRIBUTION STATEMENT (of this Report)

Approved for public release; distribution unlimited.

17. DISTRIBUTION STATEMENT (of the abstract entered in Block 20, if different from Report)

18. SUPPLEMENTARY NOTES

19. KEY WORDS (Continue on reverse side if necessary and identify by block number)

air-to-air tracking
depressed roll axis

20. ABSTRACT (Continue on reverse side if necessary and identify by block number)

A nonlinear simulation and a linear model are developed for an air-to-air tracking task using the A-7D DIGITAC aircraft. The nonlinear simulation includes the aircraft, flight control syste, target dynamics, and the relative kinematics between the aircraft and the target.

The linear model represents the linearized lateral-directional aircraft dynamics, the heading angle, and the linearized lateral relative kinematics.

DD FORM
1 JAN 73 1473   EDITION OF 1 NOV 65 IS OBSOLETE

20. (con't)
The models were used to describe the effect of depressing the aircraft roll axis on the air-to-air tracking task using a fixed gunsight.

A flight test program was conducted to determine the effects of depressing the aircraft roll axis on the lateral directional dynamics and on the air-to-air tracking task. Comparison of the flight test and nonlinear model data showed good correlation for both the mechanical flight control system and the standard control augmentation system. The linear air-to-air tracking model did not agree with flight test data due to lack of a control system in the model.

END

FILMED

3-84

DTIC